Classical Trajectory Monte Carlo Simulation of Ion-Rydberg Atom Collisions

By

Jun Lu

Dissertation for the Doctor Degree

at

University of Bielefeld

Faculty of Physics

May 2003

1. Research Supervisor: Herr Prof. Dr. Hans O. Lutz
2. First Reader: Herr Priv. Doz. Dr. Dirk Feldmann

Date of the Disputation: 2003

Table of Contents

Abstract

The aim of this work is to investigate the dynamics of collisions between ions and Rydberg atoms by using the Classical Trajectory Monte Carlo (CTMC) method. The study is started by collisions with oriented elliptical Rydberg atom, is then continued to collisions involving hydrogen Rydberg target in an external magnetic field in the l-mixing regime, and later arrives at antihydrogen formation in an external magnetic field where Rydberg positronium is taken as target.

The CTMC method has been applied in the study. For different targets, the CTMC method had to be adjusted and reconstructed to properly create the initial target state for the quasi-separable one-body initial system (hydrogen target) and the two-body initial system (positronium target). Charge exchange and ionization cross sections are calculated under special consideration of different initial target states.

The velocity matching phenomenon and Thomas capture which appears in the upstream-downstream asymmetry are found in ion-oriented elliptical Rydberg atom collisions, reflecting the important roles of the initial electron spatial and momentum distributions. By increasing the projectile charge, the distortion of the initial states caused by the strong perturbation of approaching projectile induces pronounced changes in the momentum distribution.

In the collisions involving hydrogen Rydberg atoms in a magnetic field, a cross section reduction in case of an increasing magnetic field is found for multiply charged projectiles. The structure effect due to the influence of the magnetic field on the initial state distribution results in different capture cross sections for two characterized, k_{max}

and k_{min}, states. The velocity matching phenomenon as well as the effect of multiply charged projectile ion are observed in the collisions.

Furthermore, antihydrogen formation in a magnetic field has been studied. Rydberg positroniums are assumed to be the target atoms, colliding with antiprotons. The initial target positronium state is carefully constructed by means of a newly introduced conserved operator, the pseudomomentum **K**. Similar properties as in the previous hydrogen target atom case were investigated. It is found that the existence of the magnetic field changes the spatial distribution of positronium to irregular motion. By increasing the magnetic field, it induces a decrease of the resulting capture cross sections (i.e. the antihydrogen formation). Thomas capture which happens in the collision plane in the field-free case is foiled. A smaller positronium binding energy and a larger geometrical extension of the target positronium atom yield a larger capture cross section.

Acknowledgements

I would like to thank Prof. Dr. Hans O. Lutz, my supervisor, for his constant scientific support and his many stimulating suggestions during this research. I am also thankful to Dr. Z. Roller-Lutz for her guidance through all the years of my study.

Dr. Emil Sidky supplied me with fruitful discussions about modeling of Positronium system in an external magnetic field, many valuable references. Prof. Dr. Jan Petter Hansen provided his knowledge of CTMC method, which is crucial to the successful completion of this research. I also thank Dr. Michail Zhuravlev and Prof. Dr. Nikolay Kabachnik for many most helpful and valuable discussions concerning the mathematical and computational aspects of the present work.

I had the pleasure of meeting Prof. Dr. Yongkui Zou. His support and friendship make research like this possible.

I am grateful to my family for their patience and *love*. Without them this work would never have come into existence.

Bielefeld, Germany Jun Lu

May, 2003

Introduction

Laser excitation and field ionization have enabled preparation and detection of Rydberg sublevels of definite principal quantum number n and angular momentum l [1, 2, 3, 4]. With the development of experimental techniques, it is now possible to prepare Rydberg atoms in aligned and oriented coherent elliptic states. The use of coherent elliptical Rydberg states in ion-atom collision studies has been investigated in many experiments [5, 6, 7, 8, 9, 10, 11]. The experiments that measure electron capture by heavy singly charged ions from oriented and aligned Rydberg atom have revealed much about the Coulomb three-body dynamics. They have demonstrated that velocity matching and the Thomas capture mechanism [12, 13] between the projectile and the electron are the important features of these rearrangement collisions. These investigations have so far been restricted to collisions with singly charged ions. Recently, however, it has become possible to employ such collisions in studies involving multiply charged ions [11]. Some CTMC calculations [14, 15] of electron capture by singly charged ions from oriented elliptical Rydberg atoms have been performed. These results were in agreement with the experimental data of Ehrenreich et al. [8]. The classical trajectory Monte Carlo (CTMC) method is a successful model for ion-atom collision based on classical mechanics and is briefly reviewed in chapter 1. This

method is expected to be a good approximation particular for large quantum numbers [16] and is quite useful for the description of quantum-mechanically complex systems. It has been successfully used in ion-atom collisions [16, 17, 18, 19, 20] and given a good qualitative and often fairly quantitative agreement with experimental data [11, 21, 22]. Therefore in chapter 2, an exploratory study of such three-body systems has been performed, in which a spatially oriented Rydberg atom collides with a multiply charged ion. The classical trajectory Monte Carlo (CTMC) method is employed to calculate electron capture and ionization cross-section at intermediate impact velocities for the collisions between highly charged ($Q \leq 8$) Sodium(Na) ions and hydrogen Rydberg Lithium(Li) atoms ($n = 25$). In order to study the velocity matching phenomenon and show the effect of the spatial orientation of the target electron in the multiply charged ion-Rydberg atom collisions, impact parallel to the minor and to the major axis, respectively, of the initial Kepler electron ellipse has been investigated.

At the same time, the behavior of interacting particle systems in a strong homogeneous magnetic field has become a subject of great interest. Quantum chaos and the influence of external magnetic fields on the atoms are the main research interests. The study of this behavior was in the beginning mainly motivated by the astrophysical discovery of huge magnetic fields in the vicinity of white dwarf stars ($B \approx 10^2 - 10^5$T) and neutron stars ($B \approx 10^7 - 10^9$T). The first few investigations considered only the low-lying states of hydrogen atoms under such extreme conditions. There have been a few calculations for ion-atom collisions at such field strengths [23, 24, 25, 26]. It has been shown [27] that by considering equal Coulomb and Lorentz forces for an

electron in a circular Bohr orbit with principal quantum number n,

$$B_n = \frac{B_0}{2n^3} \approx \frac{4.7 \times 10^5 T}{2n^3} \approx 8.3(\frac{30}{n})^3 T$$

is obtained as a rough measure, where $B_0 = 2\alpha^2 m_e^2 c^2/(e\hbar) \approx 4.70108 \times 10^5$T is the reference magnetic field strength. B_n scales with the inverse cube of the principal quantum number n. Thus for white dwarf and neutron star magnetic fields, lowing-lying states are found to be significantly influenced by these fields, while at laboratory field strengths studies of the strong-field regime must concentrate on Rydberg states. With the rapid improvement of computer techniques, it was possible to calculate the eigenvalues and eigenfunctions of the hydrogen atom up to the field-free ionization threshold. The magnetic energies in the highly excited Rydberg states are at typical laboratory magnetic field strengths (a few tesla) attainable and comparable or even larger than the Coulomb binding energies. It is therefore possible to study the intermediate and high-field regime by investigating highly excited states. Some calculations of electron capture and ionization for singly charged ion-Rydberg atom collisions in a magnetic field have been performed [28, 29, 30]. The target atom in these works was the simplest physical system, the hydrogen atom. It was treated as an effective one-body problem with the approximation of an infinitely heavy nucleus. To investigate more details of such collisions as well as the influence of an external magnetic field, multiply charged ions were applied to collide with Rydberg atoms at the same strengths of magnetic fields as in the works [28, 29, 30]. In chapter 3, with the extended CTMC method which has been successfully used for collision systems involving singly charged ion-Rydberg atom collisions in the magnetic field, the charge exchange and ionization cross section for $1.27 - 183eV$ singly and multiply charged Argon(Ar) ions (Q = 1, 2, 4 and 8) colliding with Rydberg Sodium(Na) atoms

($n = 28, m = 2$) in a magnetic field (B) of up to 4T have been calculated. The initial state distribution of the target atom is generated for a quasi-separable initial-state Hamiltonian. The existing magnetic field shows its influence on the resulting cross sections, which is similar to those found in the previous calculations [28, 29, 30]. The strong long-range Coulomb attraction of the increasing projectile charge dominates over the influence of the target electron distribution in these collisions.

Another interesting system, in which the "infinitely heavy" nucleus is replaced by a light particle, is positronium (Ps) e^+e^-. The study of this system is motivated by the recent success of experiments to produce significant numbers of cold antihydrogen atoms, which has opened a new door to study the fundamental symmetries in physics. Antihydrogen formation can be caused by e^+ capture from positronium, $\bar{p} + (e^+e^-) \rightarrow \bar{H} + e^-$, where the positronium can become stable in a magnetic field. Theoretical calculations on positronium in magnetic fields at laboratory field strengths have predicted the existence of long-lived states [31]. Therefore, based upon the work on ion-Rydberg atom collision in the magnetic field [29, 32], we extended our study to antihydrogen formation by collisions of antiprotons with Rydberg positronium(Ps) in a magnetic field of up to 5 Tesla. However, unlike the hydrogen atom in the magnetic field, the positronium in the magnetic field can not be treated as a quasi-one-body system, since in general the center-of-mass motion and the internal motion of the system can not be separated due to the finite e^+ mass. The first rigorous treatment of the two-body system in a magnetic field has been done by Avron, Herbst, and Simon [33]. A new operator, the pseudomomentum $\mathbf{K}$, has been introduced to perform a so-called pseudoseparation and is taken to treat the two-body problem. This pseudoseparation is connected with the center-of-mass motion, leading

to a Hamiltonian which possesses a constant of motion. The results of Avon, Herbst and Simon have been applied in many publications [34, 35, 36, 37, 38, 39, 40, 41, 42] and successfully described the dynamical behavior of the two-body system in a magnetic field. In chapter 4, the dynamics of the collision between antiproton($\bar{p}$) and Rydberg positronium(Ps) in the magnetic field $B = 4$T and 5T, leading to formation of antihydrogen($\bar{H}$), $\bar{p} + Ps \rightarrow \bar{H} + e^-$, are studied. Positronium with high principal quantum number $n = 40$ and 50 can exist in long-lived delocalized excited states, so called outer well states, which have been predicted to be formed in a magnetic field at typical laboratory field strength and certain values of the pseudomomentum. The most important part of this problem, generating the proper initial target positronium state at the presence of a magnetic field, is successfully constructed by means of the pseudomomentum $\mathbf{K}$ and is described in detail. The charge exchange cross sections (i.e. the antihydrogen formation) as a function of relative impact projectile velocity are calculated for the pseudomomenta $K = 0.085, 0.09$ and 0.12 by applying the modified CTMC method. The relative impact projectile velocity v_r is between 0.5 and 2.8 ($v_r = v/v_e$, with v_e the classical electron velocity in a field-free circular Ps Bohr orbit), corresponding collision energies between 0.62 and 19.6eV ($n = 50$) and between 0.98 and 30.6eV ($n = 40$).

Finally, chapter 5 presents a discussion of the calculated results and some conclusions. The obtained results reveal that the magnetic field as well as the increasing projectile charge take an important role in these collisions. The application of the CTMC method in the collisions of antihydrogen formation also provides us an alternative way to study the production of the antimatter atom. Furthermore, the suggestion of future objectives are given in the end.

In addition, some results are published and are attached at the end of this thesis. Atomic units ($\hbar = e = m_e = 1$) are used throughout unless specified.

Chapter 1

Theoretical Approaches to Ion-Rydberg Atom Collisions

Considerable progress has been made in past decades in the theoretical description of collisions involving Rydberg atoms. In the case that one atom is highly excited, the most effective approaches are based on a "three-body picture". In this picture, the ionic projectile is treated as a point charged particle and the Rydberg target atom is treated as a point core with the Rydberg electron orbiting around it. The size of the electron orbital is quite large relative to the dimensions of the core and the electron is therefore singled out. The scattering is performed by modeling the interactions among the electron, the target nucleus and the projectile ion.

The physical picture is that the electron begins in a large, classical elliptical orbit. As the charged ion travels through the Rydberg atom, the shape of the electron's orbit is then changed. The processes discussed here are

$$A^*(nlm) + B^+ = \begin{cases} A^*(n'l'm') + B^+ & \text{Excitation} \\ A^+ + B^*(n'l'm') & \text{Charge exchange} \\ A^+ + B^+ + e^- & \text{Ionization} \end{cases}$$

where B^+ is a charged ion and A^* is a highly excited atom with main quantum

number n, orbital angular momentum l, and magnetic quantum number m. This system has been modeled successfully by considering the Coulomb forces among the three charged particles.

Once the form of the interaction potential has been adopted, the quantum mechanical theory may be formulated and a variety of approximations may be applied. However for ion-Rydberg atom collisions, in which a large number of channels are coupled, quantum mechanical and semiclassical theories can not lead to satisfactory results. Fully quantal and semi-classical calculations of cross sections usually require large-scale numerical computations which are not easy when a large basis set is required, especially when highly excited states are involved. It is also intractable to include the ionization and excitation channels in order to accurately compute the electron capture cross sections. Therefore there has always been an interest in constructing models for ion-atoms collisions based on classical mechanics which can be evaluated rapidly.

The three-body classical-trajectory Monte Carlo (CTMC) method was first proposed by Abrines and Percival [17], has previously been described in detail by Olson and Salop [18], and was optimized by Cohen [43]. It has been successfully applied to many problems [16, 44, 45]. This method is based on the numerical integration of the three-body system. The Coulomb interactions, which includes the projectile ion, the target nucleus, and an electron initially bound to the target nucleus, are included. The Rydberg atom's electron position and momentum distribution are described classically within a statistical distribution of the initial conditions. The method has the advantage that all possible processes can be included: excitation, ionization, and electron capture by the incident projectile. Becker and Mackellar [45] have improved

the description of the atomic state using a microcanonical distribution corresponding to a given state in $|n, l\rangle$. Peach et al. [46] and Reinhold and Falcon [47] have each developed more elaborate methods to replace the Coulomb interactions by a model potential for the ionic cores. Specifically, the CTMC method has also been used for oriented atoms by Kohring et al. [48] and Pascale et al. [19]. This chapter will briefly reviewed the basic principles of the CTMC method while focusing on one-electron capture collisions involving highly excited Rydberg atoms.

1.1 Classical Trajectory Monte Carlo method

The CTMC method consists of three steps: (1)the classical generation of the initial target electron distribution, (2)the numerical integration of Newton's equations of motion with Coulombic forces, and (3)the classification of the various processes after the collision.

1.1.1 Generation of the Initial State Distribution

In CTMC method a very important consideration is the classical description of the Rydberg atom's electron position and momentum distributions. Abrines and Percival [17] have shown that it is possible to use Kepler's equation of planetary motion to represent hydrogenic atoms with a randomly determined set of initial conditions. The sampling is completed by (i)fixing the binding energy E_0; (ii)choosing the eccentricity ε of the Coulombic ellipse; (iii)solving Kepler's equation for the eccentric anomaly(eccentric angle) ξ in terms of the mean anomaly α to establish the initial position and velocity on the ellipse; (iv)applying an Euler transformation with three random angles θ, ϕ and η to set up the arbitrary orientation of the ellipse.

For a given quantal state, $|n\rangle$ is specified by the binding energy $E_0(E_0 = -\frac{1}{2n^2}$ for the hydrogen atom). The additional five random sampling parameters are ε, α and θ, ϕ, η. ε is the eccentricity of the Kepler orbit, $\varepsilon^2 = 1 + 2E_0 l_c^2$, where l_c is the classical angular momentum. The classical angular momenta l_c are restrict to the interval $l \leqslant l_c \leqslant l + 1$, which is determined by the quantum mechanical angular momenta l. Thus the eccentricity ε is chosen in the interval:

$$1 + 2E_0(l+1)^2 \leqslant \varepsilon^2 \leqslant 1 + 2E_0 l^2. \tag{1.1}$$

The angle α defines a starting point on the Kepler ellipse plane and it is a parameter of the orbit proportional to time. A random distribution of α corresponds to an equal probability of the atom having any phase in its periodic motion. ξ is the eccentric angle and is determined by solving Kepler's equation

$$\alpha = \xi - \varepsilon sin\xi. \tag{1.2}$$

The initial position and momentum of the electron on the orbit are fixed by a solution of Kepler's equation (1.2). The three Euler angles θ, ϕ, η fix the plane of the orbit in space, where

$$\theta = \cos^{-1}\frac{l_z}{l}, \tag{1.3}$$

$$\phi = \cos^{-1}(\pm\frac{\mathbb{A}_z}{\varepsilon \sin\theta}), \tag{1.4}$$

$$\eta. \tag{1.5}$$

The first rotation θ about the y axis gives the electron the proper z component of angular momentum. The second rotation ϕ about the angular momentum vector $\mathbf{l}$ fixes the z component of the Runge-Lenz vector $\mathbb{A}$. The plus or minus in Eq. (1.4) indicates that the sign of $\mathbb{A}_z$ should be chosen randomly. The final rotation about

the space fixed z axis gives the randomly chosen η angle. These five parameters are distributed in the following ranges:

$$0 \leqslant \varepsilon^2 \leqslant 1,\ 0 \leqslant \alpha \leqslant 2\pi,\ -1 \leqslant cos\theta \leqslant +1,\ -\pi \leqslant \phi \leqslant +\pi,\ -\pi \leqslant \eta \leqslant +\pi.$$

Fig. 1.1 shows the geometrical structure of the collision system. The initial internal coordinates and momenta of the target electron are given by performing the rotation specified by the Euler angles θ, ϕ and η [43].

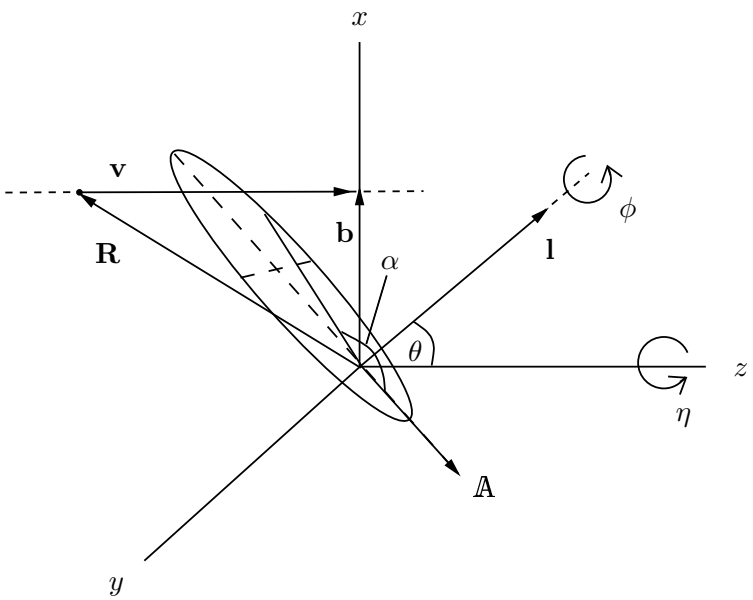

Figure 1.1: The geometry of the collision system. **R** is the internuclear vector, **b** is the impact parameter, and **v** is the ion velocity in the target frame chosen parallel with the magnetic field(z-axis), $\mathbf{R} = \mathbf{b} + \mathbf{v}t$. An example of a Kepler ellipse with the angular momentum **l** and Runge-Lenz vector $\mathbb{A}$ is also shown. The angle α which defines a point on the Kepler ellipse plane and the three Euler angles θ, ϕ, η are indicated. The dashed lines indicate the major and minor axes.

Another part of the initial condition that one must model is the incoming plane wave for the projectile ion. Here we use a standard distribution [18]. The initial

condition of the projectile in the collision frame is specified by its velocity v, its impact parameter b and its initial distance z_0 relative to the target. The z axis is chosen as the direction of the initial relative velocity vector and the projectile is assumed to move along a straight line, lying in the x-z plane. The impact parameter is selected randomly from b^2 varying in the interval $[0, b_{max}^2]$, where b_{max} is the maximum impact parameter so that negligible capture or ionization processes happen beyond this value. b_{max} depends on the target state and the ion velocity. It has to be chosen with experience for a given system. Because when b_{max} is too large, it will result in poor statistics and while a smaller value of b_{max} will distort the results. One must repeat the calculations to obtain the best b_{max} value such that the statistical error on the cross sections reduces to a reasonable level. The initial distance z_0 of the projectile is typically $z_0 > 10^4$ a.u. to guarantee that the calculated cross sections are independent of starting position. It indicates that the projectile-electron interaction is negligible compared to the target nucleus-electron interaction at the outset.

1.1.2 Numerical Integration of Newton's Equations

After propagating the initial conditions of electron, the motion of the interacting system is determined via the full three-body Hamiltonian

$$H = \sum_{i=1}^{3} \frac{p_i^2}{2m_a} + \sum_{i=4}^{6} \frac{p_i^2}{2m_b} + \sum_{i=7}^{9} \frac{p_i^2}{2m_c} + V_{ab} + V_{bc} + V_{ac} \tag{1.6}$$

and the 18 coupled Newton's classical equations of motion

$$\begin{aligned} \frac{dp_i}{dt} &= -\frac{\partial H}{\partial r_i}, \\ \frac{dr_i}{dt} &= \frac{\partial H}{\partial p_i}, \end{aligned} \tag{1.7}$$

where p_i and r_i are the momenta and the Cartesian coordinates of three particles, respectively; m_a, m_b, m_c are the masses of the projectile ion, the target atom nucleus and the electron, respectively; V_{ab}, V_{bc} and V_{ac} are the corresponding interaction potentials between two of the particles.

For each set of distribution, the Runge-Kutta method with an adaptive step-size control is applied to calculate the classical trajectories of all three bodies from a large internuclear separation to the distance of the closest approach and out again to a large internuclear separation. The initial distance z_0 of the projectile has been chosen far enough from the target that the Coulomb forces between projectile and electron are negligible compared to that between target and electron. After the three-body propagation, the projectile is at an asymptotic final distance z_f ($z_f \approx 1 \times 10^5$ a.u.). z_f is chosen such that for any position of the electron at least either the projectile-electron interaction or the target-electron interaction is negligible.

1.1.3 Classification of Final States

After each trajectory has been integrated to the distance z_f, the three-body Hamiltonian (1.6) is no longer necessary to be evolved in the particle trajectories. It is then allowed to check for reaction. By evaluating the two-body total energies of the final state, it is now possible to classify the outcome of the ion-atom collision. If, at the end of an individual trajectory, the electron is bound to the target nucleus, it is cataloged as excitation; if the electron is found to be bound to the projectile ion, the reaction is cataloged as charge exchange; and if the electron is bound to neither nucleus, it is cataloged as ionization. The cross sections for the various processes are proportional to the ratio of successful tries for that process to the number of trajectories calculated.

Generally, a large number of trajectories should be calculated in order to ensure the statistical error is less than 5%. Once a significant number of trajectories have been calculated, the cross section σ_q for a specific process q is obtained by

$$\sigma_q = \frac{N_q}{N_{tot}} \pi b_{max}^2 \left[1 \pm \sqrt{\frac{N_{tot} - N_q}{N_{tot} N_q}} \right], \tag{1.8}$$

where N_{tot} is the total number of trajectories, N_q is the number of events leading to capture or ionization. The second term in Eq. (1.8) is the standard deviation of the estimated cross section.

For the electron capture process, it is possible to 'quantize' the states corresponding to a negative binding energy E_p of the electron with respect to the projectile ionic core. A classical number n_c is defined by the hydrogenic relationship

$$E_p = -\frac{Z_p^2}{2n_c^2}, \tag{1.9}$$

where Z_p is the charge of the ionic core. The noninteger classical principal quantum number n_c is assumed to belong to the electronic level n if it lies between the values [45]

$$[(n-1)(n-\frac{1}{2})n]^{\frac{1}{3}} \leqslant n_c \leqslant [n(n+\frac{1}{2})(n+1)]^{\frac{1}{3}}. \tag{1.10}$$

Similarly, the normalized classical orbital angular momentum number l_c is 'quantize' by the orbital quantum number l of the final state if

$$l \leqslant l_c \leqslant l+1, \tag{1.11}$$

where

$$l_c = \frac{n}{n_c} |\mathbf{r} \times \mathbf{p}|, \tag{1.12}$$

$\mathbf{r}$ and $\mathbf{p}$ are the coordinate and momentum of the electron referred to the projectile ionic core, respectively.

In the same manner, the classical $m_c = (l + \frac{1}{2})/l_c^z$ corresponds to the quantum number m if it belongs to the interval $[m - \frac{1}{2}, m + \frac{1}{2}]$, where l_c^z is z component of classical angular momentum..

1.1.4 The Validity of the CTMC Method

For the problems to be treated in this work, the CTMC approach is successful for two main reasons. First, the interactions between the particles are relatively strong and long range, and final states over a wide energy range tend to be populated. The "graininess" due to the discrete energy levels of the states is therefore not too important. Second, the classical treatment of Coulomb scattering agrees with the exact quantum-mechanical approach and a statistical distribution of the initial conditions is known to be the best approach to a quantal electronic state. These considerations suggest that the CTMC approach is well suited to Rydberg atom collisions with ions or other Rydberg atoms.

The domain of validity of the CTMC method is difficult to assess and its definition mainly rests on comparisons with experimental or quantum-mechanical calculations when available. From such comparisons in $H^+ + H(1s)$ collisions, it is now generally assumed that the CTMC method is valid in the range $1 \leqslant v/v_e \leqslant 4$, where v is the projectile velocity in the laboratory frame and v_e is the initial orbital velocity of the valence electron. In Fourré and Courbin's work [20], the valid range in $H^+ + N_a^*(3p)$ collisions is $0.57 \leqslant v/v_e \leqslant 1.60$. It was suggested in [45] that when the impact speed is close to the orbital velocity of the Rydberg electron, referred to as the 'matching' speed, say $0.5 \leqslant v/v_e \leqslant 2$, the cross sections should be the most easily detectable and the most important. So we would say that for the ion-Rydberg atom collisions, the

CTMC method is a good model specially in the intermediate velocity regime where the collision velocity is approximately equal to the orbital velocity of the Rydberg atom's outer electron ($v_e = n^{-1}$ a.u.).

Chapter 2

CTMC Calculation in Collisions between Multiply Charged Ions and Elliptical Rydberg Atoms

The use of coherent elliptical Rydberg states in ion-atom collision studies [11, 21, 22] has not only aided the intuitive understanding of the interaction dynamics, it also illuminates the roles of the momentum and the spatial distributions of the target electron states. In classical terms, the *momentum distribution* can be widely varied simply by changing the eccentricity ε of the Rydberg ellipse without affecting the energy of the state. In particular, for impact perpendicular to the major axis of the ellipse, the capture cross section displays a maximum if $\mathbf{v}_{ep}$ (the perihelion electron velocity) is parallel and equal to the projectile velocity $\mathbf{v}$. This is believed to be due to the matching electron momenta in the initial target and the final projectile state. In contrast, the role of the *spatial distribution* becomes most clearly visible if the impact velocity vector is adjusted perpendicular to the minor axis of the Rydberg ellipse. In this case, the electrons can be located either between the approaching ion and the target nucleus ("upstream geometry") or behind the target nucleus, as seen from

the projectile ("downstream geometry") without otherwise changing the momentum distribution of the Rydberg state (i.e., its angular momentum l and the principal quantum number n). The capture cross section in both cases turns out to be quite different: it is much larger in the upstream case as compared to the downstream case. Apparently, in the corresponding region of parameter space the spatial characteristics of the initial state determine the outcome of the collision. An investigation of such systems, which is not only restricted to the collisions with singly charged ions, but is also extended to the collisions between the spatially oriented Rydberg atom and the multiply charged ions. This investigation is performed using CTMC method in this chapter. We may suspect that the increasing projectile ion charge, which has the strong long-range attraction over the initial target distribution, plays an importance role in the collisions and causes an increasing cross section.

The process here is structureless Sodium(Na) ions of charge Q between 1 and 8 colliding with Rydberg target Lithium(Li) atoms with nuclear charge $q = 1$ and principal quantum number $n = 25$, i.e.

$$Na^{+Q} + Li\,(n = 25) \Rightarrow Na^{+Q-1} + Li^{+}. \tag{2.1}$$

For simplicity, we ignore the cores of the collision partners, and approximate the system by $H^+ + H(n = 25) \rightarrow H + H^+$. The geometry is chosen such that the direction of impact is perpendicular to the angular momentum direction of the Kepler ellipse. Specifically, two cases are studied: (i)the impact is parallel to the minor axis, thus allowing to study the velocity matching phenomenon, and (ii)impact parallel to the major axis, showing the effect of the spatial orientation of the target electron ("upstream-downstream asymmetry").

A useful quantity characterizing the electron orbit is the (generalized) eccentricity $\varepsilon = \pm\sqrt{1-(l/n)^2}$. For the present calculation, the desired shape and spatial orientation of the elliptical states have been chosen by properly adjusting the Euler angles and the eccentricity. The relative collision velocities v_r are between 0.3 and 3.0 ($v_r = v/v_e$ with v the projectile ion velocity and $v_e = 1/n(a.u.)$ the classical electron velocity of a circular Rydberg state having the principal quantum number n). Under the consideration of the relative speed of the projectile ion and the target atom, and the lightness of the electron compared to the atomic nuclei, for the multiply charged Na ion colliding with a Rydberg Li atom, the target nucleus is taken to remain motionless. It has been tested that there is almost no effect when the target nucleus is motional for hydrogen-like atom and at the same time it saves computation time. The projectile is assumed to move along a straight line at a constant velocity $\mathbf{v}$. Due to the spatial extension of the electron state and the corresponding large impact parameter, this is a good approximation. The number of trajectories was adjusted to obtain statistical uncertainties are less than 5%. Care has been taken to assure that the projectile starts sufficiently far from the target (approximately $z_0 = 3.5 \times 10^5$ atomic units a.u.) to correctly describe the initial part of the trajectory. In view of the long range Coulomb potential and the known sensitivity of Rydberg states to l, m changing processes, this is critical particularly for higher projectile charges Q.

2.1 Impact Parallel to the Minor Axis

In this case, the target nucleus rests at the coordinate origin. The classical electron ellipse lies close to the x-z plane, with the major axis parallel to the x axis (perihelion at positive x) and the minor axis parallel to the z axis. The quantum mechanical space

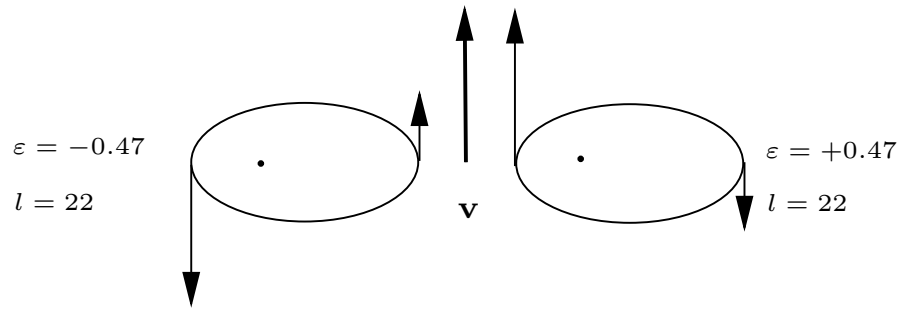

Figure 2.1: Schematic representation of the classical electron orbit with generalized eccentricities $\varepsilon = \pm 0.47$, corresponding to $l = 22$, relative to the projectile motion $\mathbf{v}$.

and momentum distribution of an l, m state are simulated by randomly selecting the classical l_c, m_c values between l and $l+1$, m and $m+1$, respectively. The projectile moves on a nearly straight line along the z-direction. The projectile velocity $\mathbf{v}$ is chosen to be parallel or antiparallel to the electron perihelion velocity $\mathbf{v_{ep}}$ (Fig. 2.1). The positive ε identifies orbits with $\mathbf{v}$ parallel to $\mathbf{v_{ep}}$ and the negative ε identifies orbits with $\mathbf{v}$ antiparallel to $\mathbf{v_{ep}}$.

Figure 2.2 shows the eccentricity dependent charge exchange cross section σ/Q for $v_r = 1.66$ and Q ranging from 1 to 8. Velocity matching is obtained at $\varepsilon = +0.47$. At low Q, the cross section displays the well-known velocity-matching behavior [15] with a pronounced maximum at this eccentricity and a deep minimum for negative eccentricities which characterize a strongly elongated Kepler ellipse with $\mathbf{v}$ antiparallel to $\mathbf{v_{ep}}$. At increasing Q, this structure is soon washed out; while it is still noticeable for Q=2 and 4, almost any trace of the minimum has disappeared for Q=8. Inspection of electron trajectories during the approach of the projectile ion reveals that: as expected, the long range Coulomb force distorts the original Kepler ellipse already at

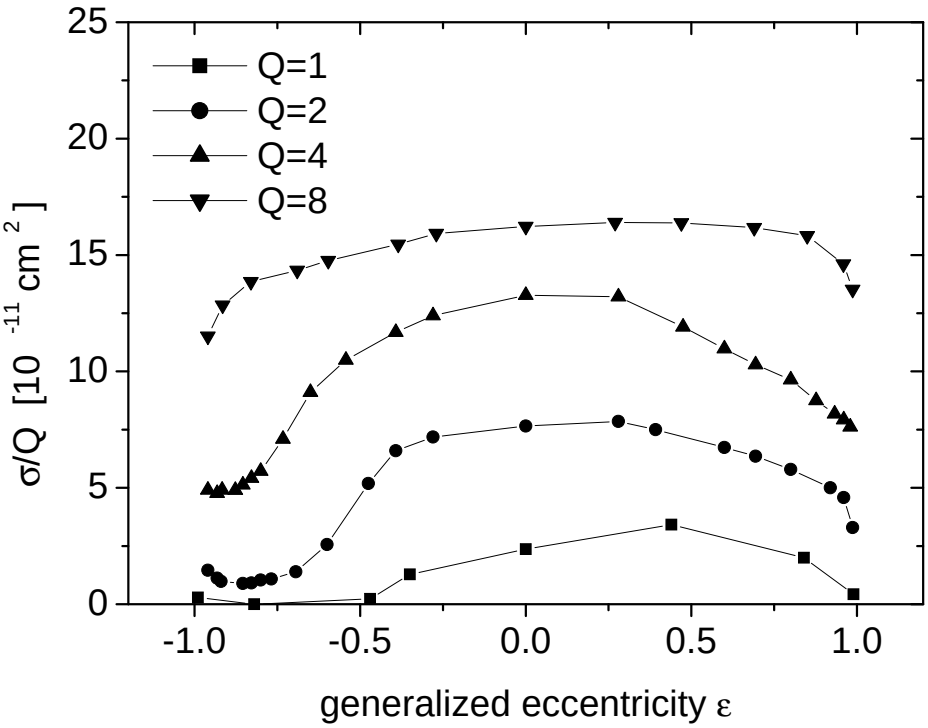

Figure 2.2: Eccentricity dependent charge exchange cross section σ/Q for impact velocity $v_r = 1.66$ (in units of the circular $n = 25$ Rydberg electron velocity) and different projectile charges Q. Impact is parallel to the minor axis. For the initial state, velocity matching is obtained at $\varepsilon = +0.47$.

quite long distances. This distortion is quite regular, and reminds of a Stark effect. Indeed, a simple estimate confirms that: for Q=8, an electric field strength of 5V/cm (i.e., of the order of the fields applied to the collision region in the experiments [11]) is attained at approximately 10^5 a.u. This initial state effect might be reduced in the experiment by applying a strong field in the target region. However, this result also illuminates an inherent weakness of the CTMC-approach: the slow rise of the electric field may "in reality" induce adiabatic transitions between the many Rydberg states which would be populated differently in the classical calculation. This distortion of

the initial state becomes quite severe at distances below 10^4 a.u., i.e., corresponding to several revolution of the Rydberg electron about its nucleus.

Therefore, it is to be believed that the washing out of the cross section structure is indeed a real effect. Finally, it may be added that the impact parameter dependence of the capture probability also reflects the signature of this effect. While, for Q=1 and $\varepsilon = +0.47$ (the velocity matching situation), the capture probability is rather concentrated about the perihelion position [15], it is nearly symmetric about b=0 (the position of the target nucleus) for Q=8.

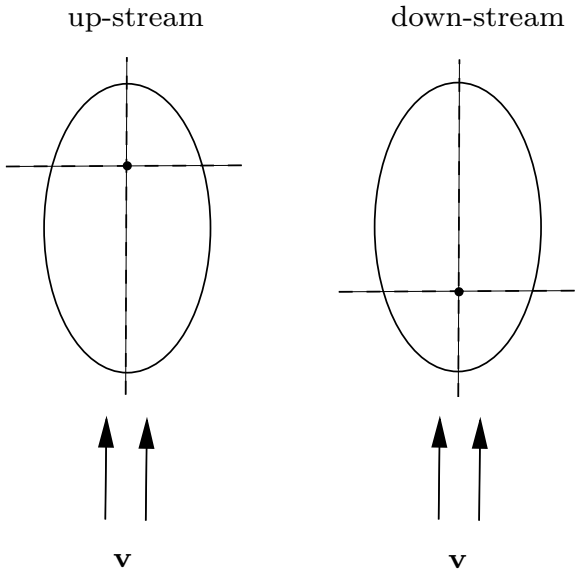

Figure 2.3: Schematic representation of the classical electron orbits of up-stream and downstream geometries, relative to the projectile motion **v**.

2.2 Impact Parallel to the Major Axis

In this case, the classical electron ellipse lies close to the x-z plane, but with the major axis parallel to the z axis and the minor axis parallel to the x axis. The electron ellipse

is located either in the upstream geometry or downstream geometry. The positive ε in this case characterizes the upstream geometry and the negative ε characterizes the downstream geometry (cf. Fig. 2.3).

Figure 2.4 shows the eccentricity dependent capture cross section σ/Q for $v_r = 1.66$. As in case of singly charged projectiles Q=1 [21], the cross section for multiply charged ions (Q=2, 4 and 8) is much higher for the upstream geometry as compared to the downstream geometry. The ellipses with $\varepsilon = \pm\ 0.96$, corresponding to $l = 7$, are chosen for a more detailed study. This creates quite elongated states which are not too non-classical (low l). Fig. 2.5 shows for Q=8 the cross sections for upstream (σ_u) and downstream (σ_d) geometry, respectively, including the contributions of the various "swaps" to the capture cross sections. A swap has been defined as a passage of the electron through the "midplane" between projectile and the target nucleus [9]. Note, however, that for asymmetric collisions ($q \neq Q$ as studied here), this plane cuts the connection line between target and projectile nucleus at the saddle point of the two respective Coulomb potentials (i.e, at a distance $R/(1 + \sqrt{q/Q})$ from the projectile, with R the distance of both nuclei). For $q \neq Q$, the so-called "midplan" is not really in the middle. In view of the discussion above, the strong upstream-downstream asymmetry observed in these data is at first glance somewhat surprising. Again, inspection of the electron trajectories sheds light on this point: the slowly increasing electric field of the approaching projectile causes a distortion and precession of the Kepler ellipse, in general not strong enough, however, to revert the upstream into a downstream geometry and *vice versa*. Therefore, upon approach of the projectile into the actual close interaction the electron is still mainly fore or aft, respectively, of the target nucleus. Thus the role of the initial spatial distribution of the electron

is qualitatively preserved . Interestingly, even 3-swap and higher swap processes can still be discerned. The qualitatively different behavior of σ_u and σ_d beyond $v_r = 1.5$ is associated with differently rising cross sections for ionization. In case of downstream geometry it sets in at considerably smaller v_r-values as compared to the upstream geometry. This is further clarified by the respective impact parameter dependencies (Fig. 2.6 a,b). In the upstream situation, charge exchange extends out to fairly large distances and ionization is still weak. In the downstream situation, the maximum charge exchange probability is of the same order as in the upstream case, however, it is limited to much smaller impact parameters, and ionization is already quite strong.

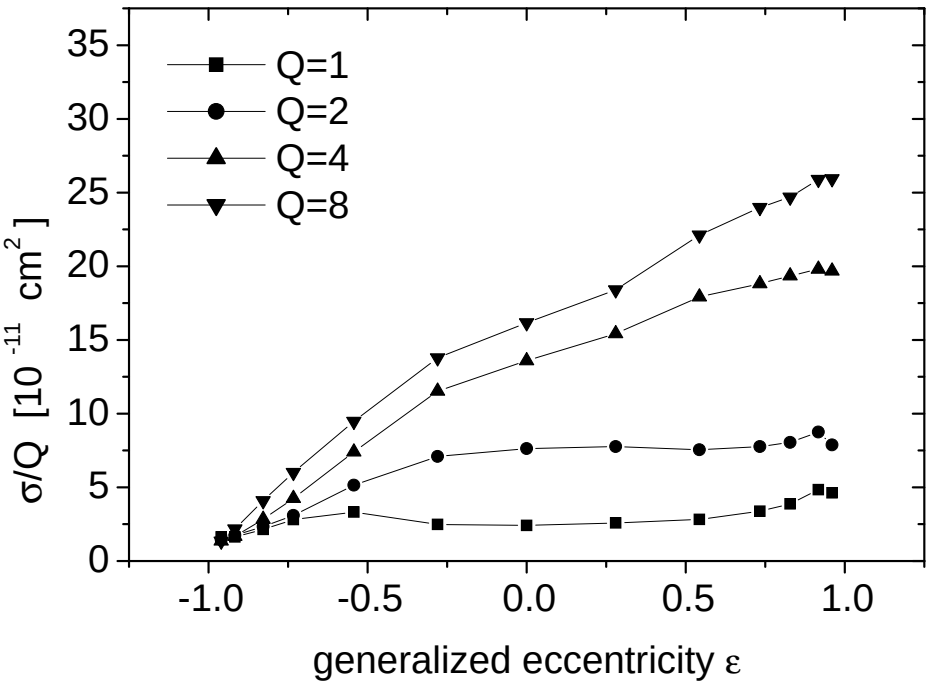

Figure 2.4: Eccentricity dependent charge exchange cross section σ/Q for impact velocity $v_r = 1.66$ and different projectile charges Q. Impact is parallel to the major axis, $\varepsilon > 0$ (< 0) correspond to the upstream (downstream) geometry.

From the above calculations and analysis, it shows that for impact of multiply

charged ions of intermediate velocities the role of the initial electron momentum distribution becomes weaker for increasing projectile charge. This is due to the strong perturbation of the initial state by the approaching ion which induces pronounced changes in the momentum distribution long before the actual close interaction occurs. In contrast, the initial spatial orientation of the electron continues to be important for all Q-values studied here.

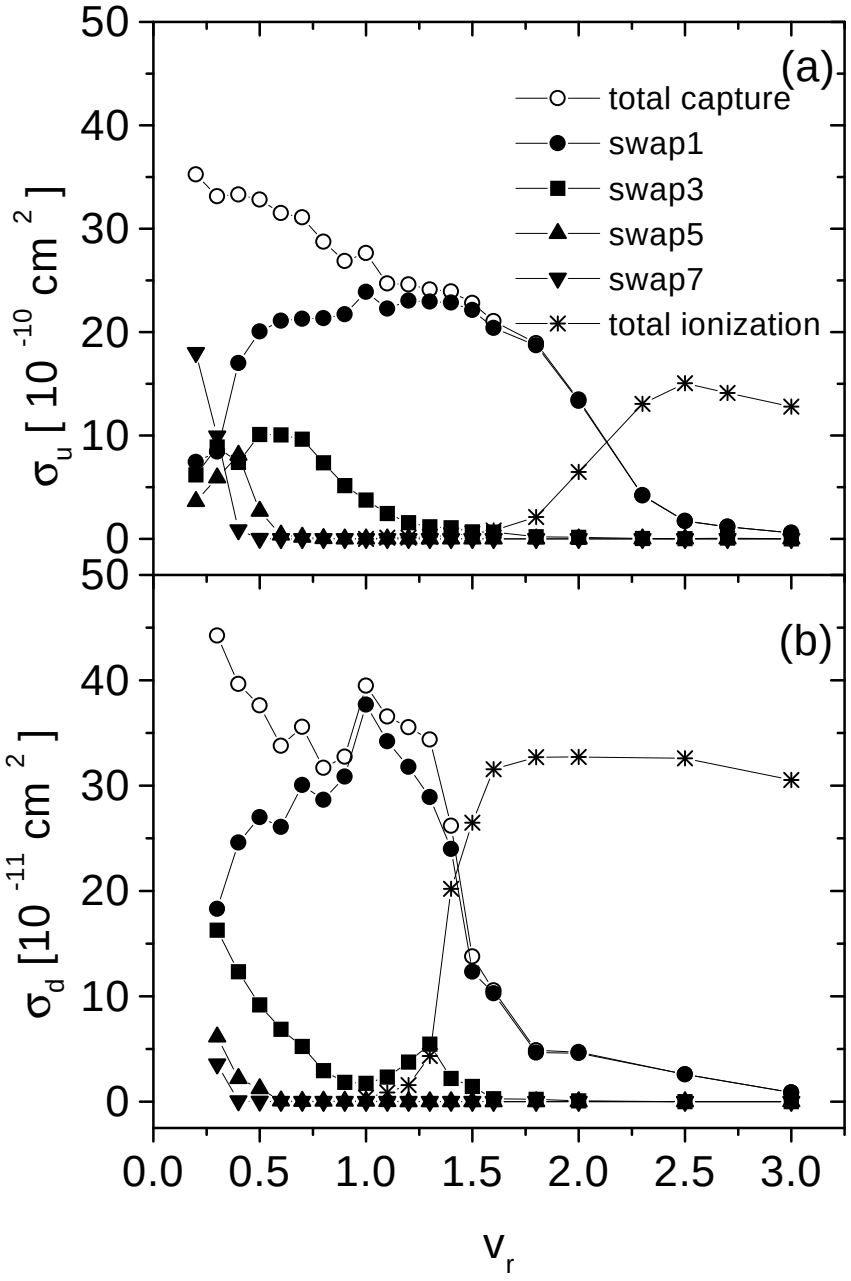

Figure 2.5: Charge exchange cross sections (Q=8) for (a) upstream σ_u and (b) downstream σ_d geometry; the eccentricity $\varepsilon = \pm 0.96$. The respective ionization cross sections are also given.

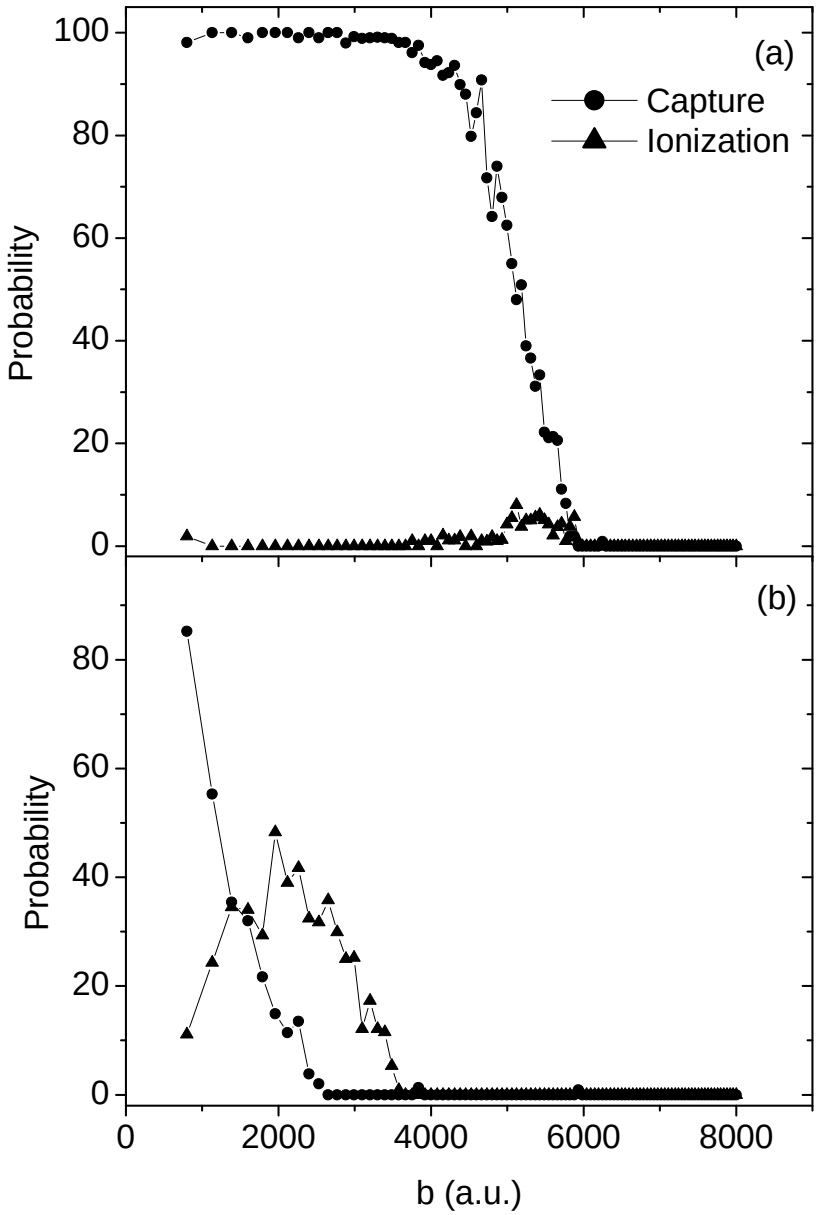

Figure 2.6: Impact parameter dependent probabilities of capture and ionization: (a) upstream geometry, (b) downstream geometry. Impact parameter b in atomic units; impact velocity $v_r = 1.5$; projectile charge $Q = 8$.

Chapter 3

Extended CTMC to Electron Capture in Multiply Charged Ion-Rydberg Atom Collisions in an External Magnetic Field

The CTMC method is successfully applied for the separable initial-state problem in chapter 2. For the particular system that the hydrogen-like target atom stays in a magnetic field, the problem is compounded by the non-integrable initial state, which means that all three steps in the CTMC method need to be modified. In the following sections, a novel method for generating the starting distribution for a quasi-separable initial-state Hamiltonian is presented. With this extended CTMC method, the charge exchange cross sections for the collisions between multiply charged ions and Rydberg atoms in the l-mixing magnetic field regime are carried out.

3.1 The Rydberg Atom in a Magnetic Field

First let us look at the behavior of a hydrogen-like Rydberg atom in the magnetic field. In classical mechanics, the effect of a magnetic field on the Hamiltonian of a

particle of charge $-e$ can be obtained by replacing the linear momentum $\mathbf{p}$ by $\mathbf{p}+e\mathbf{A}$, where $\mathbf{A}$ is the vector potential of the field. The Hamiltonian of an electron moving in a potential $V(r)$ and a magnetic field $\mathbf{B}$ is then

$$H = \frac{1}{2}(\mathbf{p} + \mathbf{A})^2 + V(r), \tag{3.1}$$

where $\mathbf{B} = \nabla \times \mathbf{A}$. For our problem the Coulomb symmetric gauge ($\nabla \cdot \mathbf{A} = 0$) is chosen, and for a uniform field along the z axis, $\mathbf{A} = (\mathbf{B} \times \mathbf{r})/2$.

To understand the structure in fields where the diamagnetic interaction plays the principal role, we shall display the Hamiltonian

$$H = H_{ke} + H_{coul} + H_{para} + H_{dia}, \tag{3.2}$$

where H_{ke} denotes the terms involving only the kinetic energy of the electron, H_{coul} denotes the Coulomb interaction between particles, H_{para} denotes the orbital paramagnetic interaction and H_{dia} denotes the diamagnetic interaction. The electron spin-orbit, spin-spin and the nuclear spin interactions are not considered in this work. For the different strengths of magnetic field, various regimes may be distinguished:

- $H_{dia} << H_{coul}$: the ordinary Zeeman-effect, diamagnetic term is negligible.
- $H_{dia} < H_{coul}$: l-mixing regime, diamagnetic term is small but not negligible. l is not a good quantum number.
- $H_{dia} \approx H_{coul}$: intermediate field regime, diamagnetic term is comparable to the Coulomb terms. n is not a good quantum number.
- $H_{dia} >> H_{coul}$: Landau regime. The Coulomb interaction is treated as a perturbation. The free-electron problem is taken as the starting point.

In this study, for a Rydberg atom state $n = 28$, $m = 2$ in a magnetic field of up to 4T, the ratio of magnetic energy to Coulomb energy is of the order 0.1. It is the case of l-mixing regime and therefore n is still a good quantum number. The l-mixing regime is experimentally accessible and perturbation theory is applicable.

3.2 Multiply Charged Ion-Rydberg Atom Collisions in a Magnetic Field

The process under study is the Ar ions of charge Q between 1 and 8 colliding with Rydberg Na atoms in a magnetic field of up to 4T, i.e.

$$Ar^{+Q} + Na\,(n = 28, m = 2) \Rightarrow Ar^{+Q-1} + Na^{+}. \tag{3.3}$$

As in the previous chapter, we ignore the cores of the collision partners. The hydrogen-like atom Na is assumed to have an "infinitely heavy" proton nucleus, which is treated as a one-body system and is quasi-separable in a magnetic field. The Hamiltonian governing the electron trajectory in a magnetic field is

$$H = \frac{\mathbf{p}^2}{2} - \frac{1}{|\mathbf{r}|} - \frac{Q}{|\mathbf{r} - \mathbf{R}|} + \frac{1}{2}\gamma l_z + \frac{1}{8}\gamma^2\rho^2, \tag{3.4}$$

where $\mathbf{R} = \mathbf{b} + \mathbf{v}t$, $\gamma = B/(2.3505{\times}10^5\text{T})$, $\rho^2 = x^2 + y^2$. l_z is the z-component of the electron angular momentum, B is the magnetic field strength expressed in tesla, $\mathbf{R}$ is the internuclear vector, $\mathbf{b}$ is the impact parameter and $\mathbf{v}$ is the projectile ion velocity in the target frame chosen parallel to the magnetic field.

In this study, the field strength was chosen such that the magnetic energy of the active electron is less than but comparable to the Coulomb energy in the field of the target nucleus. In addition, this study has been restricted to experimentally accessible

fields of up to a few tesla. Both requirements can be met if the target atoms are in Rydberg states with high principal quantum numbers n. In this work, the target atom has the principal quantum number $n = 28$ and the magnetic quantum number $m = 2$. These states can easily be prepared by laser-optical pumping. Such collision systems are at the boundary of classical and quantum mechanics. Since they are not yet accessible to a quantum-mechanical treatment, the classical trajectory Monte Carlo (CTMC) method is applied. For ion-atom collisions, this method has been made popular by the work of Olson and coworkers (cf., e.g., [49]), and is known to be quite useful in particular for quantum mechanically complex systems (as, for example, Rydberg atom collisions). With the ratio of magnetic energy to target atom Coulomb energy of the order 0.1, n and m are still good quantum numbers, but the electron angular momentum l is no longer, the diamagnetic energy is taken as a perturbation. For the l-mixing region degenerate perturbation theory reveals quantum eigenstates of the diamagnetic Rydberg atom [50]. The manifold of eigenstates that emerge from the diagonalization of the diamagnetic potential split into two types of states, which are characterized by a new quantum number k. Those corresponding to the high set of energy eigen values ϵ_k with low k values are perpendicular to the magnetic field and the lower-energy states (high k) resemble the states being elongated along the magnetic field z-axis. For the states with $n = 28, m = 2$, one finds that $k_{max} = 24$ and $k_{min} = 0$, since k must correspond to an even parity state. The state with minimum value $k_{min} = 0$ corresponds to a disk-shape state and is somewhat similar to the field-free $l = m = 2$ state. And the state with maximum value $k_{max} = 24$, corresponds to a cigar-shape state.

The calculations are from singly charged ion impact (Q=1) to ion charges Q = 2,

4 and 8 at magnetic field strengths of 0, 2 and 4T, respectively. The collision energies (between 1.27 and 183 eV) correspond to impact velocities v_r between 0.2 and 2.4 ($v_r = v/v_e$, with v_e the classical electron velocity in a circular $n = 28$ orbit).

3.2.1 Initial State Distribution

Generating the initial-state distribution is one of the main challenges of the CTMC method. Based on the results of the quantum mechanical [50, 51] and classical [52] perturbation theories for a Rydberg atom in a magnetic field, an extended CTMC method [28] for generating a stationary microcanonical ensemble for a quasi-integrable one-body initial-state Hamiltonian is briefly presented here.

At the presence of a magnetic field, a quasi-integrable initial-state Hamiltonian for a stationary Rydberg atom is

$$H_{init} = H_0 + U \tag{3.5}$$

where

$$H_0 = \frac{1}{2}\mathbf{p}^2 - \frac{1}{|\mathbf{r}|} + \frac{1}{2}\gamma l_z, \tag{3.6}$$

and

$$U = \frac{1}{8}\gamma^2\rho^2 \tag{3.7}$$

H_0 represents the Rydberg atom under the linear Zeeman effect which is integrable and U is the diamagnetic interaction which is treated as a small perturbation introducing nonseparability into H_{init}. The magnitude of U is small enough that the classical orbits of H_{init} are still regular. The diamagnetic interaction causes a slow drift of the angular momentum vector $\mathbb{l}$ and Runge-Lenz vector $\mathbb{A}$. The resulting electron orbit is thus a combination of the fast elliptical motion, an intermediate

cyclotron motion and a slow oscillation (magnetron motion with period τ_{mag}) of the elliptical parameters. Unlike the pure elliptical motion, the new orbit is not closed. As has been shown in classical perturbation theory [52], an approximate constant of motion $\Lambda = 4|\mathbb{A}|^2 - 5\mathbb{A}_z^2$ emerges. $\mathbb{A}_z$ is the z component of the Runge-Lenz vector $\mathbb{A}$. Orbits corresponding to negative values of Λ are stretched along the magnetic field as with the high k values from the quantum mechanical perturbation theory, and positive Λ correspond to the low k values, i.e., a disklike distribution perpendicular to the magnetic field. The magnetron period τ_{mag} for a given k state is calculated by numerically integrating Eq. (5) in [52] with $\Lambda = (\epsilon - n^2 - m^2)/n^2$ [51].

In practice the electron is randomly placed on an ellipse oriented in the coordinate x-y plane with the aphelion on the negative x axis. The size and shape of the ellipse are determined by the angular momentum l and the eccentricity ε. The starting point on the ellipse is chosen by selecting a mean anomaly α in $[0, 2\pi]$, where α determines the Kepler anomaly ξ through Keplers equation (Eq. (1.2)). The proper orientation is accomplished by three rotations through the three Euler angles (cf. Eqs. (1.3), (1.4), (1.5)).

After the procedures stated above, the electrons are distributed over the perturbed orbit with a probability inversely proportional to the electron speed. The electron phase-space coordinates are evolved according to equation $H_{init} = H_0 + U$ for a time randomly varying between 0 and τ_{mag}.

Due to the diamagnetic term, an unperturbed ellipse would not give the correct total energy and the particles in the ensemble world have different energies contradicting one of the basic tenets of CTMC calculations [17, 18]. Therefore, for each starting point the angular momentum is adjusted slightly resulting in a new ellipse

and a different diamagnetic energy (cf. Eq. (2.18) in [29]). After 10 recursions of this correction the electron energy has a relative error 10^{-7} of the quantum mechanical binding energy, and the constants of motion are preserved.

3.2.2 Integration of Hamilton's Equations of Motion

After the generation of the initial positions, the integration of the Hamiltion equations of motion (Eq. (1.7)) according to the three-body Hamiltonian (Eq. (3.4)) are carried out with the projectile starting at $z_0 (z_0 \geqslant 5.0 \times 10^5)$ and ending at $z_f (z_f \approx 2 \times 10^5)$. The approximation of fixed target nucleus and a straight line projectile trajectory with constant velocity is taken similarly as in chapter 2.

3.2.3 Final-state Classification

When it is not necessary to evolve the particle trajectories under the full three-body Hamiltonian equation (Eq. (3.4)), while propagating the electron trajectory with the two-body Hamiltonians, the two-body interaction energies of electron-target H_{e-T} and of electron-projectile H_{e-p} are calculated,

$$H_{e-p} = \frac{1}{2}(\mathbf{p} - \mathbf{v})^2 - \frac{Q}{|\mathbf{r} - \mathbf{R}|} + \frac{1}{2}\gamma l_z + \frac{1}{8}\gamma^2\rho^2 \tag{3.8}$$

$$H_{e-T} = H_{init} \tag{3.9}$$

where both are expressed in the target frame. Evaluation of these energies allows the classification of the outcome of the ion-atom collision. Since l_z is a good quantum number, for H_{e-T}, the ionization threshold is $\frac{1}{2}\gamma(|l_z| + l_z)$ due to the combined effect of the centrifugal and diamagnetic potentials. If H_{e-T} is constant and less than $\frac{1}{2}\gamma(|l_z| + l_z)$, the electron remains bound to the target nucleus. For H_{e-p}, the ionization threshold is zero. If H_{e-p} is constant and less that zero, the electron has been captured

by the projectile nucleus. All other situations when the two-body system breaks up lead to ionization.

3.3 Results

The resulting velocity dependent charge exchange cross sections for k_{max} and k_{min} states are shown in Fig. 3.1 and Fig. 3.2. Two effects can be seen: i)an external magnetic field reduces the cross sections, and ii)an increase of the projectile charge washes out the structures observed in the cross sections of $Q = 1$.

3.3.1 B-dependence

The cross section reduction in case of an increasing magnetic field has already been found for singly charged projectiles [28]. We may recall that the influence of the field is twofold: it alters the initial electron state distribution('structure effect') as well as the charge exchange dynamics. The structure effect can be separated by looking at the difference between the k_{max} and the k_{min} cross sections for B=0. It contains the influence of the initial state momentum distribution (i.e., the effect of the matching velocities of the projectile and the captured electron) as well as their spatial extension. Although the structure effect appears to be somewhat reduced for increasing Q (cf. the B=0 curves in Fig. 3.3), at B=4T the k_{max} cross section is still significantly shifted to higher v_r compared to the k_{min} cross section. This shift has been interpreted as a signature of the velocity matching effect [28]: the strong z-momentum components in the cigar-shaped k_{max}-state facilitate capture at higher impact velocities. The $Q = 2$ and Q =4 projectiles yield a behavior between $Q = 1$ and $Q = 8$.

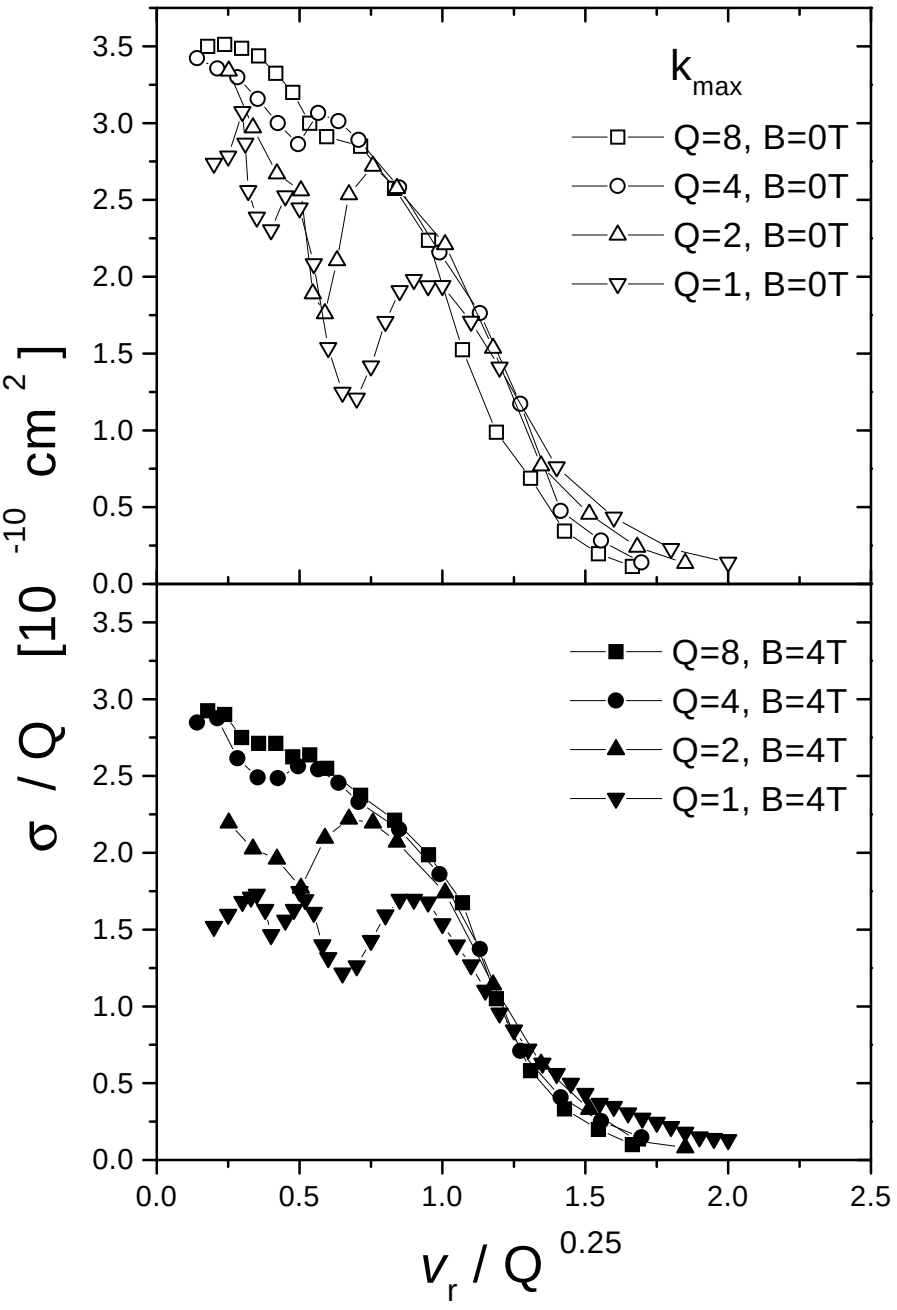

Figure 3.1: Velocity dependent charge exchange cross section for collisions of Q-fold ionized projectiles with targets in the k_{max} initial state. Top: field-free condition ($B = 0T$); bottom: external magnetic field ($B = 4T$).

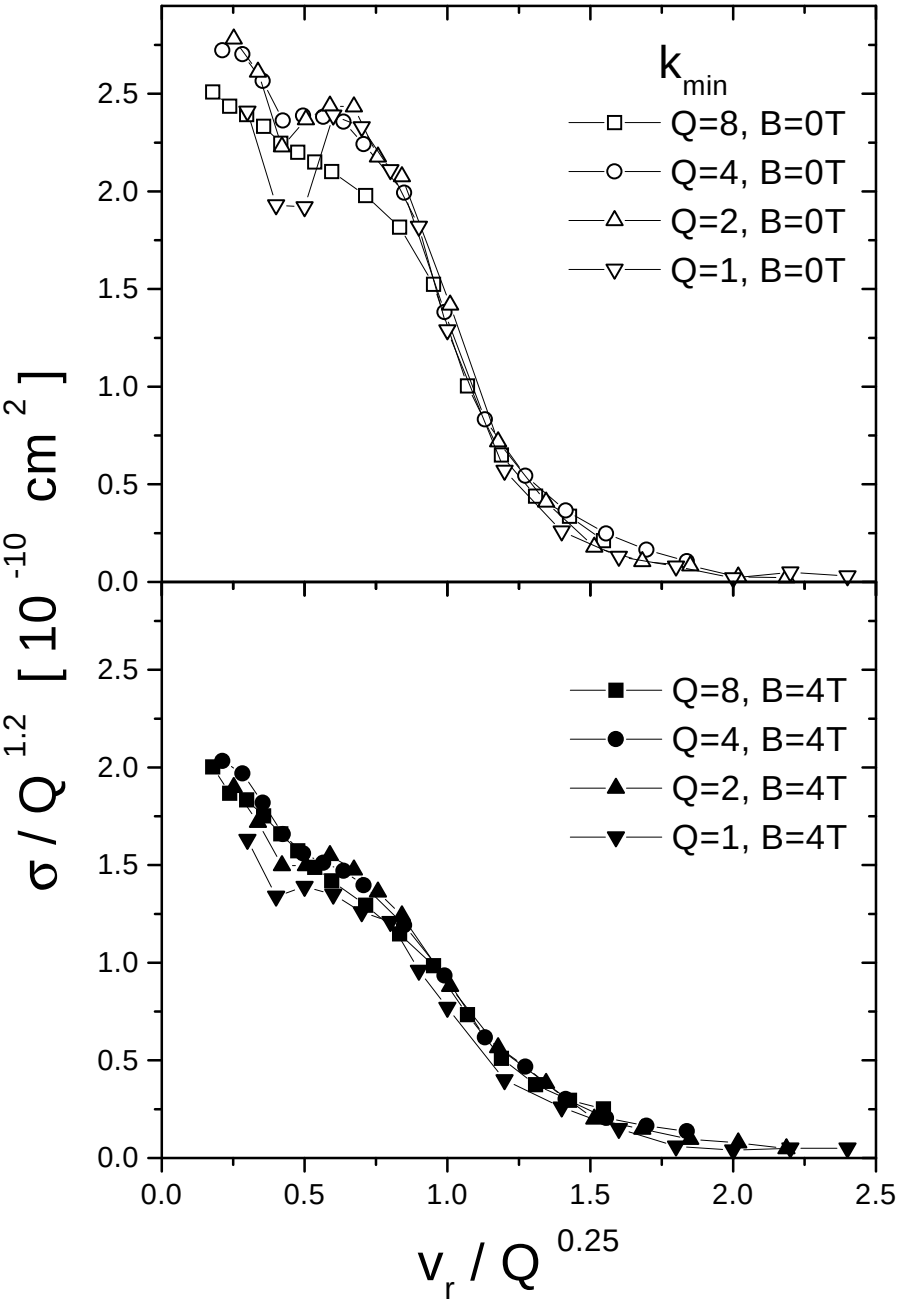

Figure 3.2: Velocity dependent charge exchange cross section for collisions of Q-fold ionized projectiles with targets in the k_{min} initial state. Top: field-free condition ($B = 0T$); bottom: external magnetic field ($B = 4T$).

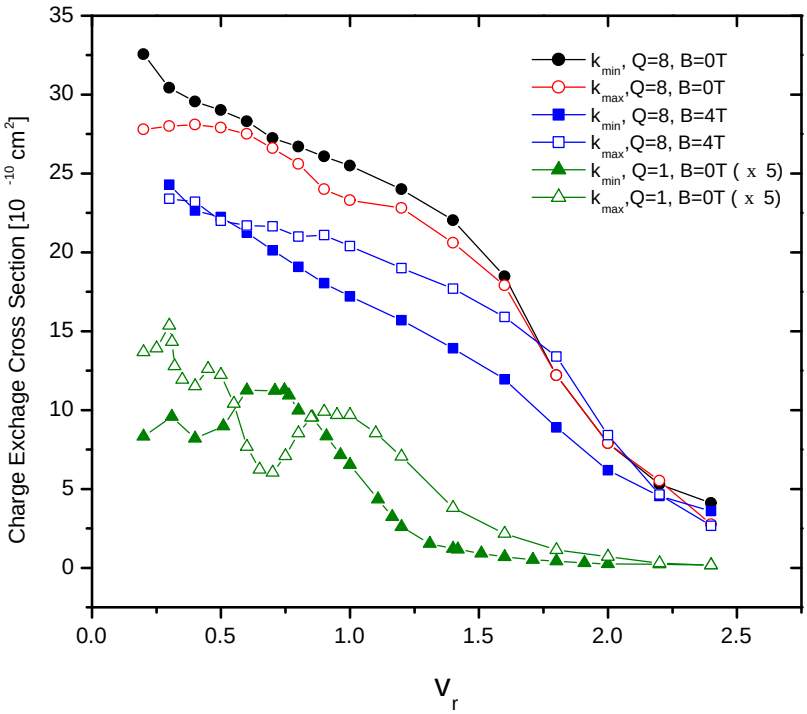

Figure 3.3: Comparison of k_{min} and k_{max} cross sections for different projectile charge and magnetic field.

3.3.2 Q-dependence

Following the references [53, 54], σ/Q^{α} and $v_r/Q^{0.25}$ have been chosen as semi-empirical scaling quantities in Fig. 3.1 and Fig. 3.2. For the k_{max} initial state $\alpha \approx 1$, while $\alpha \approx 1.2$ gives a somewhat better fit in case of k_{min}.

Particularly pronounced deviations from the simple scaling in Fig. 3.1 and Fig. 3.2 show up at $v_r < 1$. The cross section structure at these velocities has been attributed to the so-called "swaps" [9, 21, 28]; the effect of $q \neq Q$ has been considered

here similar to that in chapter 2. The order of swaps characterizes how often the electron passes through the "midplane" before it finally stays with the projectile. As an example, Fig. 3.4 displays the contributions of the various swaps to the k_{min}-charge exchange cross section when the projectile is singly ($Q = 1$) or highly charged ($Q = 8$); k_{max} behaves qualitatively similar. Compared to $Q = 1$ the contributions of the various swaps to $Q = 8$ spread over wider velocity increments, and the swap structure is washed out. Evidently, the reason is that for increasing Q the strong long-range Coulomb attraction increasingly dominates over the influence of different target electron distributions. One may expect that this is a general phenomenon which should be observed also in other alignment and orientation studies with highly charged ions.

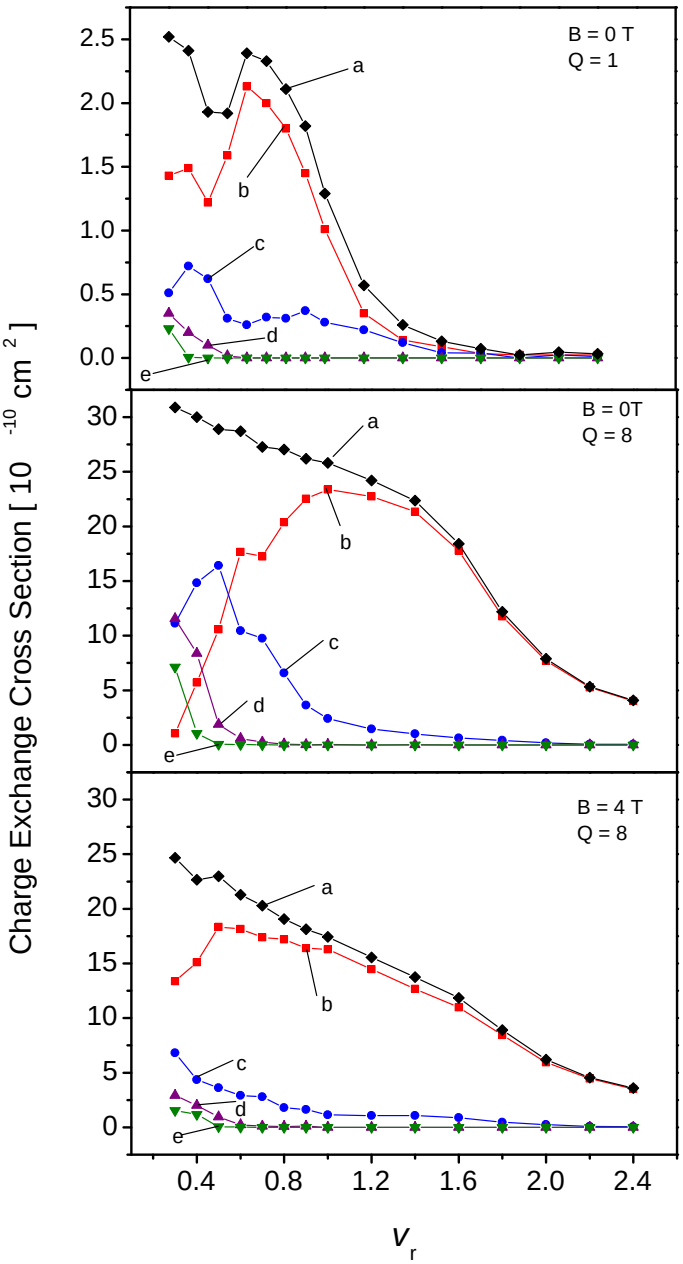

Figure 3.4: Contributions of "swaps" to the total charge exchange cross section(a) for k_{min} initial target states: 1 swap(b), 3 swaps(c), 5 swaps(d), 7 swaps(e).

Chapter 4

Modified CTMC to Antiproton-Positronium Collisions in an External Magnetic Field

In the previous chapters, the behavior of a simple physical system, the hydrogen Rydberg atom in a magnetic field colliding with an ion, has been studied in detail. The initial state was treated as an effective one-body problem. Another interesting target system is positronium, consisting of two light particles. The research on this system is motivated by the recent success of experiments [55, 56, 57, 58, 59] to produce significant numbers of cold antihydrogen atoms. It has opened a new door to a test of the fundamental symmetries in physics. An accurate spectrometry of photon transitions in hydrogen and its antiparticle could resolve the question if the Rydberg constants in both systems are identical, as required by the CPT theorem. In these experiments, positrons from a radioactive source are moderated in a W foil, capture an electron and form highly excited Ps. This Ps is then field-ionized, yielding cold positrons in a trap. Cold antihydrogen is produced when slow antiprotons are repeatedly driven into collisions with cold positrons stored in the "nested trap". Three-particle $\bar{p} - 2e^+$

recombination as well as radiative $\bar{p} - e^+$ recombination are discussed as possible causes for antihydrogen formation. However, as an alternative route also e^+ capture from positronium,

$$\bar{p} + (e^+e^-) \Rightarrow \bar{H} + e^- \tag{4.1}$$

has recently received considerable attention (cf. [60, 61] and references therein). For all these processes, a major problem in the quantitative interpretation of the experimental results lies in the unknown effect of the strong (≈ 5 Tesla) magnetic field in the trap. Therefore, previously reported large charge exchange cross sections in collisions between hydrogen Rydberg atoms and protons in an external magnetic field [32] suggest to produce antihydrogen atoms by collisions of antiprotons $\bar{p}$ with Rydberg positronium in a magnetic field of up to 5 Tesla (Eq. (4.1)). We want to study the effects of the magnetic field on $\bar{p} - Ps$ collisions. Our study may also provide a first-step model to estimate the influence of the external magnetic field on the $\bar{p} - 2e^+$ system. Both situations deal with a three-body collision involving two weakly interacting light particles, trapped at large distances from each other about their respective magnetic field lines.

The presence of a magnetic field in such calculations is by no means a trivial problem since in general the center-of-mass motion and the internal motion of the system cannot be separated. Unlike the previous hydrogen Rydberg target atom which was treated as an effective one-body problem, for the positronium(Ps) in a magnetic field a one-body treatment is not available. However the theoretical efforts on the treatment of two-body effect in external fields which arise due to the finite nuclear mass show us a way to work more precisely on such interacting particles in the magnetic field. The first rigorous treatment of a two-body system in a magnetic

field has been published by Avron, Herbst and Simon [33]. A new operator connected with the center-of-mass motion, the so-called pseudomomentum **K**, was introduced in their work. It represents a conserved quantity for the system, making it possible for neutral systems to perform a pseudoseparation of the center-of-mass motion. The results of Avon, Herbst and Simon fully described the dynamics of the two-body system and have been used in many publications [34, 35, 36, 37, 38, 39, 40, 41, 42].

The target positronium in $\bar{p}-e^+e^-$ collisions is a special case of the two-body system and is of great interest in theoretical and experimental investigations. A classical investigation of the highly excited positronium [31, 62] atom in a magnetic field has been performed by Schmelcher, Cederbaum and coworkers. Long-lived excited states of positronium have been predicted to be formed in a magnetic field at laboratory field strengths [31]. The behavior of the two-body system was fully taken into account, and all effects due to the finite masses have been considered. It was shown [42, 63, 64] that the kinetic energy of the center-of-mass motion can be interpreted as part of the effective potential for the internal motion of the neutral two-particle system. This effective potential is gauge independent and distorted by the magnetic field. Above a critical value of the pseudomomentum K_c, an additional potential well forms on the negative x axis and will be referred to as the outer well (OW). The outer well moves away from the magnetically distorted Coulomb potential and becomes broader and deeper with increasing K. Particles in this OW are trapped at large distances from each other, leading to delocalized states. They are stable and undisturbed.

In this chapter, the theoretical method and numerical calculation of charge exchange cross sections as a function of relative impact projectile velocity for the reaction $\bar{p} + Ps \rightarrow \bar{H} + e^-$ are presented. The target positronium atoms, embedded

in magnetic fields of 4T and 5T, are in Rydberg states with binding energies corresponding to field-free principal quantum number $n = 40$ and 50. We concentrate on the outer well state with values of pseudomomentum K around 0.1, which are above the critical value. Thus, long lived delocalized outer well states are formed. Collision energies of the antiproton range from 0.62 to 19.6eV ($n = 50$) and from 0.98 to 30.6eV ($n = 40$).

4.1 Theoretical Approach

To calculate the cross section for the reaction $\bar{p} + Ps \rightarrow \bar{H} + e^-$ in a magnetic field, the modified CTMC method which has been adjusted for the positronium target is applied. The generation of the initial positronium state is the main challenge in this work. In contrast to the hydrogen Rydberg atom with an "infinitely heavy" proton nucleus, the unstable center-of-mass of positronium in a magnetic field makes a direct application of the established CTMC method more difficult to generate the target particle distribution under study here. We follow the treatment proposed by the Heidelberg group [31, 42, 62] to construct the initial distribution of the target particles. This process is different from the previous method for the hydrogen atom system. In the following sections, the construction of initial states of positronium in a homogeneous magnetic field is given according to the center-of-mass pseudoseparation introduced by Avron, Herbst and Simon [33]. For those long-lived delocalized outer well states, which are the main basis of this study, the anisotropic harmonic oscillator approximation (AHO) [42, 63] is used to expand the potential well around its minimum.

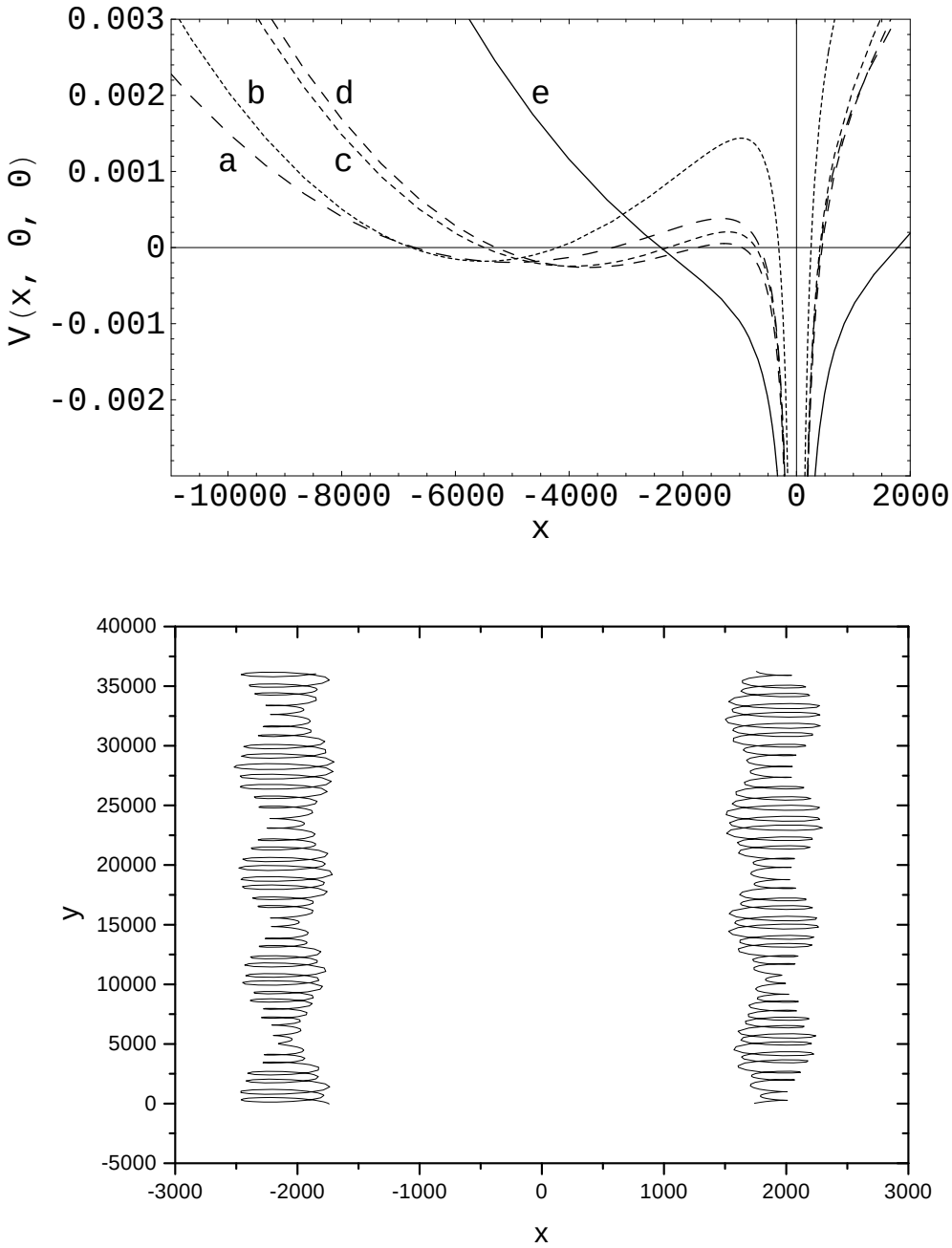

Figure 4.1: Top: $V(x,0,0)$ for Ps in a magnetic field. a: $B = 4T, K = 0.09$, b: $B = 5T, K = 0.12$, c: $B = 5T, K = 0.09$, d: $B = 5T, K = 0.085$, e: $B = 5T, K = 0.01$; Solid curve: $K < K_c$, for all other curves $K > K_c$. x is the particle distance perpendicular to the field direction. Bottom: One example of particle trajectories of Ps in the external magnetic field $B = 5$T, $n = 50$ and $K = 0.09$. The magnetic field points along the z-direction.

4.1.1 Positronium in a Homogeneous Magnetic Field

Considering the equal masses and opposite charges of positronium constituents, the Hamiltonian of two particles in a homogeneous magnetic field is given by

$$H_{Ps} = \frac{1}{2}(\mathbf{p}_1 + \mathbf{A}_1)^2 + \frac{1}{2}(\mathbf{p}_2 - \mathbf{A}_2)^2 - \frac{1}{\mid \mathbf{r}_1 - \mathbf{r}_2 \mid}, \tag{4.2}$$

where $\mathbf{p_1}, \mathbf{p_2}$ and $\mathbf{r_1}, \mathbf{r_2}$ are the momenta and coordinates of the electron and positron, respectively. $\mathbf{A}_1 = \frac{1}{2}\mathbf{B} \times \mathbf{r_1}$ and $\mathbf{A_2} = \frac{1}{2}\mathbf{B} \times \mathbf{r_2}$ are the symmetric vector potentials of the two particles. The Hamiltonian of Eq. (4.2) is not translationally invariant and the total momentum is not conserved. However, the pseudomomentum

$$\mathbf{K} = \mathbf{p_1} + \mathbf{p_2} - \frac{\mathbf{1}}{\mathbf{2}}\mathbf{B} \times \mathbf{r_1} + \frac{\mathbf{1}}{\mathbf{2}}\mathbf{B} \times \mathbf{r_2} \tag{4.3}$$

is a conserved quantity for the system [31] and is introduced to perform a pseudoseparation of the center-of-mass motion.

For the special case of positronium, the effective Hamiltonian associated with internal motion and pseudomomentum is given in Cartesian coordinates by

$$H_{Ps} = \frac{1}{2\mu}\mathbf{p}^2 + \frac{\gamma^2}{4}(x^2 + y^2) + \frac{\gamma K x}{2} + \frac{K^2}{4} - \frac{1}{\mid \mathbf{r} \mid}, \tag{4.4}$$

where $\mathbf{r} = \mathbf{r_1} - \mathbf{r_2}$ and $\mathbf{p} = \mathbf{p_1} - \mathbf{p_2}$ are the interparticle distance and momentum vectors, respectively. $\mid \mathbf{r} \mid = \sqrt{x^2 + y^2 + z^2}$, and μ is the reduced mass. The magnetic field vector is $\mathbf{B} = (0, 0, \gamma)$, where $\gamma = \dfrac{B\,(\text{Tesla})}{2.35 \times 10^5}$. The pseudomomentum vector $\mathbf{K} = (0, K, 0)$ is assumed to point along the y-axis. The effective potential in the H_{Ps} is

$$V = \frac{\gamma^2}{4}(x^2 + y^2) + \frac{\gamma K x}{2} + \frac{K^2}{4} - \frac{1}{\sqrt{x^2 + y^2 + z^2}}. \tag{4.5}$$

For each fixed B, the shape of the potential well changes for increasing K (see Fig. 4.1). In addition to the Coulomb singularity $V(0, 0, 0) = -\infty$, for sufficiently large K

(Above a critical value $K = K_c = \sqrt[3]{27B/2}$ [31]) the potential has a local minimum $V_0 = V(x_0, 0, 0)$ (with $x_0 < 0$) which is the so called outer well. The outer well is separated from the magnetically distorted Coulomb well (MDCW) by the saddle $V_s = V(x_s, 0, 0)$. For fixed B, some general features of the potential are observed:

- The value of x_0 decreases with increasing K; the outer well moves away from MDCW along the negative x axis.
- The minimum of the outer well V_0 moves upwards with increasing K but is bounded from above by zero.
- The value of x_s increases with increasing K; the barrier maximum moves towards the origin.
- The height of the saddle V_s increases without limit with increasing K.

The outer well states are also called delocalized states because the average interparticle separation is large. For $K > K_c$, the outer well becomes broader and deeper with increasing K. For the problems we are studying, when $B = 4T$, $K_c = 0.0612$ and $B = 5T$, $K_c = 0.066$. For a field-free Rydberg state $n = 50$, we have chosen $B = 4$T, $K = 0.12$ and $B = 5$T, $K = 0.09$; For a state $n = 40$, we have chosen $B = 5$T, $K = 0.085$. The three pseudomomenta are above the corresponding critical values. Thus, outer wells are formed which we approximate by an anisotropic harmonic oscillator and expand around the minimum. The resulting long-lived delocalized OW states are the required initial target states. Fig. 4.1 shows examples of the potential well for positronium, the cases of interest in this work. The bound states in the outer well are bounded from above by the ionization threshold and below by the well

minimum. E.g., for $B = 5T, K = 0.09, n = 50$ the minimum of the outer well is at $x_0 = -3947.22$.

4.1.2 Initial States Construction of Target Positronium

To define the initial position and momentum of the positronium in the outer well state, we need to specify 12 quantities in the position and momentum vectors:

$$\begin{aligned} \mathbf{r}_1 &= (x_1, y_1, z_1), \quad \mathbf{p}_1 = (p_{x1}, p_{y1}, p_{z1}), \\ \mathbf{r}_2 &= (x_2, y_2, z_2), \quad \mathbf{p}_2 = (p_{x2}, p_{y2}, p_{z2}). \end{aligned} \tag{4.6}$$

With the definition in Eq. (4.3) and $\mathbf{K} = (0, K, 0)$, we obtain

$$\begin{aligned} p_{x1} + p_{x2} + \frac{\gamma}{2}(y_1 - y_2) &= 0, \\ p_{y1} + p_{y2} - \frac{\gamma}{2}(x_1 - x_2) &= K, \\ p_{z1} + p_{z2} &= 0. \end{aligned} \tag{4.7}$$

For a given initial state, $\mathbf{r}$ and $\mathbf{p}$ are known from the harmonic oscillator approximation and are derived in the next paragraph. Through $\mathbf{r} = \mathbf{r}_1 - \mathbf{r}_2$ and $\mathbf{p} = \mathbf{p}_1 - \mathbf{p}_2$, where $\mathbf{r} = (x, y, z)$, $\mathbf{p} = (p_x, p_y, p_z)$, another 6 equations are derived

$$\begin{aligned} x_1 - x_2 &= x, \\ y_1 - y_2 &= y, \\ z_1 - z_2 &= z, \\ p_{x1} - p_{x2} &= p_x, \\ p_{y1} - p_{y2} &= p_y, \\ p_{z1} - p_{z2} &= p_z. \end{aligned} \tag{4.8}$$

In addition, the center-of-mass is initially put at the coordinate origin, which means $\mathbf{r}_1 + \mathbf{r}_2 = 0$. Therefore,

$$\begin{aligned} x_1 + x_2 &= 0, \\ y_1 + y_2 &= 0, \\ z_1 + z_2 &= 0. \end{aligned} \tag{4.9}$$

In these 12 equations, K and γ are known constants. When $\mathbf{r} = (x, y, z)$ and $\mathbf{p} = (p_x, p_y, p_z)$ are defined, the position and momentum of the initial state are easily constructed.

The initial $\mathbf{r}$ and $\mathbf{p}$ are constructed in terms of the harmonic oscillator approximation. The construction starts from the bottom of the outer well because we know that at the potential minimum V_0, the kinetic energy is maximum. We may also recall that the effective potential is $V = \frac{1}{4}\gamma^2(x^2+y^2) + \frac{1}{2}\gamma K x + \frac{1}{4}K^2 - 1/\sqrt{x^2+y^2+z^2}$. By solving the equation $\partial V(x,0,0)/\partial x = 0$, the potential then has the local minimum $V_0 = V(x_0, 0, 0)$, e.g. for $B = 5T, K = 0.09$ at $x_0 = -3947.22$. The possible maximum kinetic energy E_{kmax} at the bottom of the potential well is

$$E_{kmax} = E - V_0, \tag{4.10}$$

where E is the total energy of the positronium. Consequently, the maximum momentum P_{max} is

$$P_{max} = \sqrt{2\mu E_{kmax}} = \sqrt{E_{kmax}}\,. \tag{4.11}$$

The initial momenta of internal motion of positronium distributed in x, y, z directions are

$$\begin{aligned} p_{x0} &= P_{max} sin\vartheta cos\varphi, \\ p_{y0} &= P_{max} sin\vartheta sin\varphi, \\ p_{z0} &= P_{max} cos\varphi, \end{aligned} \tag{4.12}$$

where ϑ is selected in $[0, \pi]$ and φ is in $[0, 2\pi]$.

Having the starting position at $(x_0, 0, 0)$ and the starting momentum (p_{x0}, p_{y0}, p_{z0}), the initial internal coordinates are obtained by integrating Hamiltonians H_x, H_y, H_z in three directions, where

$$H_x = \frac{1}{2}\mu p_x^2 + \frac{1}{4}\gamma^2 x^2 + \frac{\gamma K x}{2} + \frac{K^2}{4} - \frac{1}{|x|} \tag{4.13}$$

$$(x_{start} = x_0, p_{xstart} = p_{x0}, y_{start} = 0, p_{ystart} = 0, z_{start} = 0, p_{zstart} = 0),$$

$$H_y = \frac{1}{2\mu}(p_{xinit}^2 + p_y^2) + \frac{\gamma^2}{4}(x_{init}^2 + y^2) + \frac{\gamma K x_{init}}{2} + \frac{K^2}{4} - \frac{1}{\sqrt{x_{init}^2 + y^2}} \tag{4.14}$$

$$(x_{start} = x_{init}, p_{xstart} = p_{xinit}, y_{start} = 0, p_{ystart} = p_{y0}, z_{start} = 0, p_{zstart} = 0),$$

$$H_z = \frac{1}{2\mu}(p_{xinit}^2 + p_{yinit}^2 + p_z^2) + \frac{\gamma^2}{4}(x_{init}^2 + y_{init}^2) + \frac{\gamma K x_{init}}{2} + \frac{K^2}{4} - \frac{1}{\sqrt{x_{init}^2 + y_{init}^2 + z^2}} \tag{4.15}$$

$$(x_{start} = x_{init}, p_{xstart} = p_{xinit}, y_{start} = y_{init}, p_{ystart} = p_{yinit}, z_{start} = 0, p_{zstart} = p_{z0}).$$

The integrations start with $x_{start} = x_0$, $p_{xstart} = p_{x0}$, $y_{start} = 0$, $z_{start} = 0$, $p_{ystart} = 0$ and $p_{zstart} = 0$ for H_x. In y direction, the output of H_x, x_{init}, p_{xinit} are taken as the initial values of the x direction and $y_{start} = 0$, $p_{ystart} = p_{y0}$, $z_{start} = 0$, $p_{zstart} = 0$. The same procedure is applied for z direction, the output of H_x and H_y, x_{init}, p_{xinit}, y_{init}, p_{yinit} are taken as initial values for x and y direction, respectively, and $z_{start} = 0$, $p_{zstart} = p_{z0}$. The integrations evolve for a random time between 0 and periods τ_x, τ_y, τ_z in x, y, z directions, respectively.

τ_x, τ_y, τ_z are determined by the energy distributed in x, y, z directions, respectively. With the harmonic oscillator approximation, τ_x, τ_y, τ_z are calculated by

$$\begin{aligned} \frac{\tau_x}{4} &= \int_0^{x_t} \frac{1}{v_x} dx, \\ \frac{\tau_y}{4} &= \int_0^{y_t} \frac{1}{v_y} dy, \\ \frac{\tau_z}{4} &= \int_0^{z_t} \frac{1}{v_z} dz, \end{aligned} \tag{4.16}$$

where v_x, v_y, v_z are the velocities in x, y, z directions and x_t, y_t, z_t are the turning points of the harmonic oscillators in x, y, z directions, respectively. Notice that

$$\begin{aligned} \frac{1}{2}\mu v_x^2 &= E_x - V_x, \\ \frac{1}{2}\mu v_y^2 &= E_y - V_y, \\ \frac{1}{2}\mu v_z^2 &= E_z - V_z, \end{aligned} \tag{4.17}$$

where E_x, E_y, E_z, V_x, V_y, V_z are the total energies and potentials in x, y, z directions, respectively. There holds

$$\begin{aligned} v_x &= \sqrt{\frac{2}{\mu}(E_x - V_x)}, \\ v_y &= \sqrt{\frac{2}{\mu}(E_y - V_y)}, \\ v_z &= \sqrt{\frac{2}{\mu}(E_z - V_z)}\,. \end{aligned} \tag{4.18}$$

Thus, the random initial coordinates and momenta of the positronium are defined.

Figure 4.2 shows the spatial initial positions of Ps for the state $n = 50, B = 5T, K = 0.09$. Some internal coordinate distribution of the positronium ensemble are shown in Fig. 4.3, having randomly distributed starting conditions in coordinate/momentum space and serving as initial state for the collision of Ps with $\bar{p}$ at the different field strength and pseudomomentum. At the same magnetic field strength B, the internal distance $\mathbf{r}$ of the positronium increases with increasing K (cf. also Fig. 4.1), while a stronger field and a higher internal binding energy (i.e., smaller n) compress the internal distance, in agreement with Shertzer, Ackermann and Schmelcher's work [31]. For comparison, a field-free situation is also included.

The initial condition of the projectile ions is similar to that in chapter 3. Note that b_{max} depends on the target state and the ion velocity due to the center-of-mass motion of the positronium. Therefore, the origin of the impact parameters $b = 0$ is established by calculating the meeting point of the projectile and the positronium, taking into account the projectile velocity and the center-of-mass motion of the positronium. The maximum impact parameter b_{max} is chosen sufficiently large to ensure a vanishingly small capture probability outside this b-value. The initial distance z_0 of the projectile ($\gtrsim 5 \times 10^4$ $a.u.$) is chosen such that at this distance

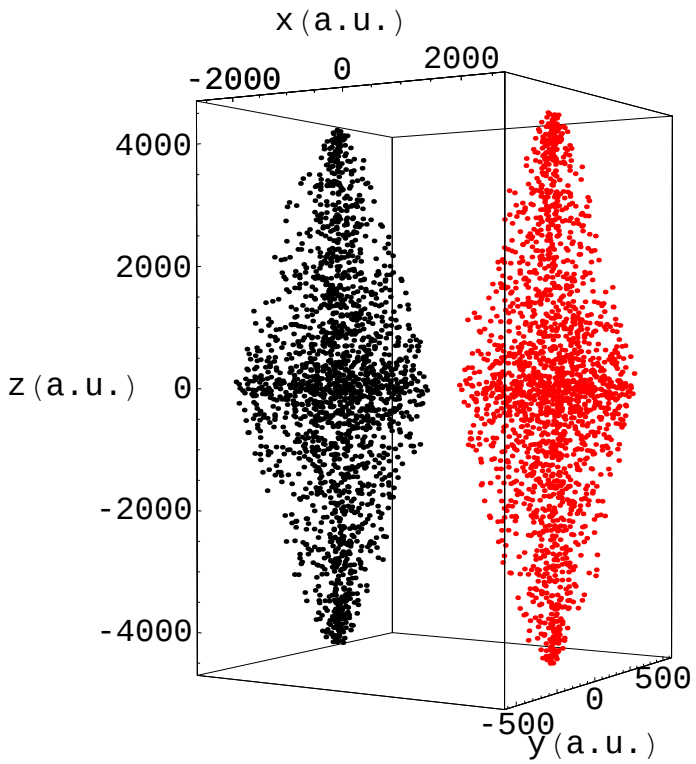

Figure 4.2: The spatial initial positions of Ps at magnetic field $B = 5$T, $n = 50$, $K = 0.09$.

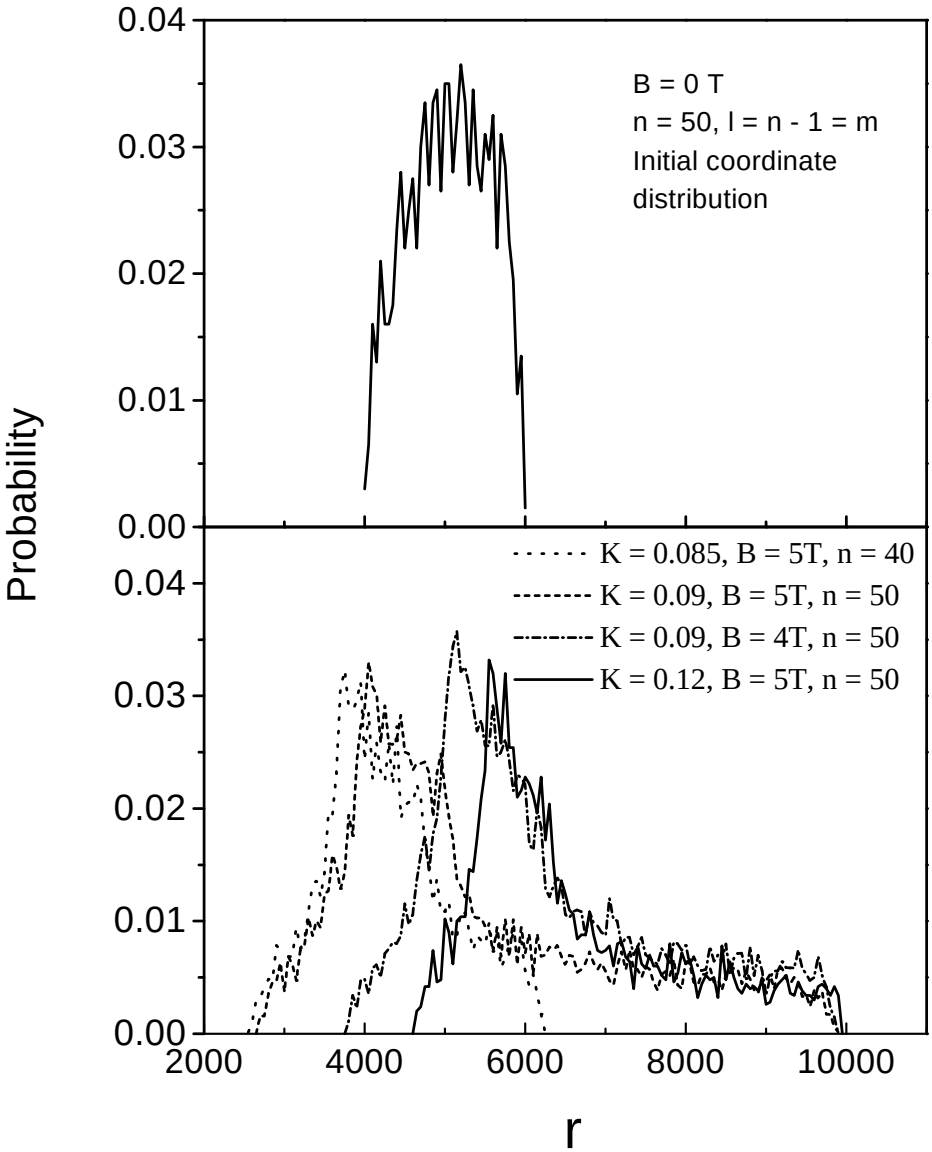

Figure 4.3: Initial coordinate distribution of the positronium ensemble. Top: field-free condition (B = 0T), $n = 50, l = n - 1 = m$; bottom: external magnetic fields B = 4T and 5T , n = 40, 50, K =0.085, 0.09 and 0.12.

the projectile-positronium interaction is negligible compared to the electron-positron interaction.

4.1.3 Integration of Hamilton's Equations

During the collisions, the projectile evolves with the approximation of a straight line projectile trajectory under the full three-body Hamiltonian,

$$H = \frac{1}{2}(\mathbf{p}_1 + \mathbf{A}_1)^2 + \frac{1}{2}(\mathbf{p}_2 - \mathbf{A}_2)^2 - \frac{1}{\mid \mathbf{r}_1 - \mathbf{r}_2 \mid} + \frac{1}{\mid \mathbf{r}_1 - \mathbf{r}_3 \mid} - \frac{1}{\mid \mathbf{r}_2 - \mathbf{r}_3 \mid}, \quad (4.19)$$

where $\mathbf{r}_3$ is the coordinate of the projectile. For a given set of initial positions, the integration of Hamilton's equations of motion (1.7) is performed according to the three-body Hamiltonian equation (4.19) by a standard Runge-Kutta method.

4.1.4 Final-state Classification

After the collision, the final asymptotic distance of the projectile z_f ($z_f = 2 \times 10^5 a.u.$) is sufficiently large to allow a clear energetic separation of the three particles into two-particle pairs. The required two-body Hamiltonians of the final states for the electron-positron pair and the positron-antiproton pair, $H_{e^+-e^-}$ and $H_{e^+-\bar{p}}$, are respectively defined by

$$H_{e^+-e^-} = \frac{1}{2}(\mathbf{p}_1 + \mathbf{A}_1)^2 + \frac{1}{2}(\mathbf{p}_2 - \mathbf{A}_2)^2 - \frac{1}{\mid \mathbf{r}_1 - \mathbf{r}_2 \mid}, \quad (4.20)$$

$$H_{e^+-\bar{p}} = \frac{1}{2}(\mathbf{p}_2 - \mathbf{v})^2 - \frac{1}{|\mathbf{r}_2 - \mathbf{r}_3|} + \frac{1}{2}\gamma l_z + \frac{1}{8}\gamma^2(x_2^2 + y_2^2), \quad (4.21)$$

where $\mathbf{v}$ is the projectile ion velocity and l_z is the z-component of the angular momentum of the e^+ angular momentum. The two-body interaction energies $H_{e^+-e^-}$ and $H_{e^+-\bar{p}}$ are calculated based on equations (4.20) and (4.21). At z_f, by evaluating

the standard deviation of both two-body energies, we may find that at least one of energies is constant in time. This evaluation of energy allows the classification of the outcome of the collision: excitation or ionization of the target positronium, or capture by the projectile ion. The ionization threshold of positronium as well as of $\bar{H}$ in the presence of the magnetic field are zero. If $H_{e^+-e^-}$ is constant and less than zero, the positron remains bound to the e^-. If $H_{e^+-\bar{p}}$ is constant and less than zero, the positron is captured by the projectile. All other situations lead to ionization.

4.2 Results

With the method outlined above, the charge exchange cross-section for the collision $Ps+\bar{p} \rightarrow \bar{H}+e^-$ in a magnetic field as a function of relative impact projectile velocity are calculated in terms of Eq. (1.8), by averaging over a great number of randomly chosen trajectories.

The initial target positronium are in $n = 40$ and 50 Rydberg states embedded in magnetic field strengths of 4T and 5 T. The impact projectile velocities v_r are between 0.5 and 2.8 ($v_r = v/v_e$, with v_e the classical electron velocity in a field-free circular Ps Bohr orbit), corresponding to collision energies between 0.62 and 19.6eV(n=50) and between 0.98 and 30.6eV(n=40). The results of the charge exchange cross section are displayed in Fig. 4.4. To illuminate the influence of the magnetic field, the cross sections for the field-free case have also been calculated. In Fig. 4.4 we include the results for two cases $l = n - 1 = m$ and $l = n - 1, m = 0$, i.e., for circular Rydberg motion in planes perpendicular and parallel to the magnetic field direction, respectively. To prove the vanishingly small charge exchange cross section outside b_{max}, Fig. 4.5 shows as an example the impact-parameter dependence for a selected

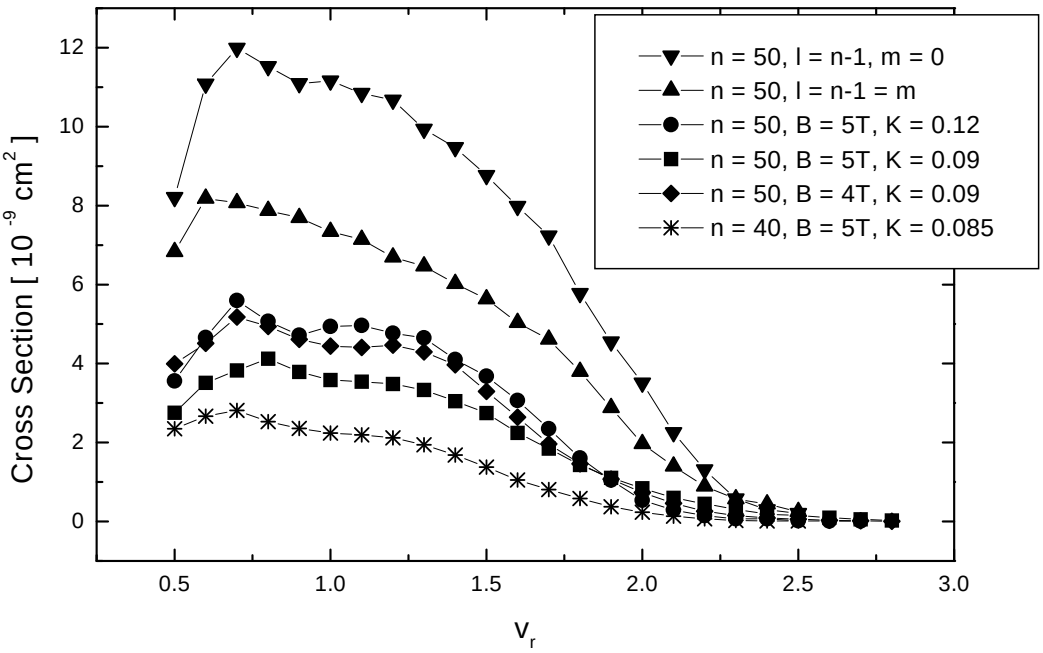

Figure 4.4: Velocity-dependent charge exchange cross section for collisions of $\bar{p}$ projectiles with Ps targets in the external magnetic fields $B = 4T, 5T$ and $n = 40, 50$ and $K = 0.085, 0.09, 0.12$ initial states, respectively. For comparison, the field-free $n = 50, l = n-1 = m$ and $l = n-1, m = 0$ initial states are also included.

velocity $v_r = 1.7$. The charge exchange probability becomes zero long before the impact-parameter extends out to b_{max}. The influence of the magnetic field is quite substantial: it reduces the cross section. The magnitude of this reduction is similar to the one observed in $p - H$ collisions [29]. A smaller positronium binding energy (increasing n) and a larger geometrical extension of the target positronium atom (increasing K) yield a larger capture cross section. This is true for $B = 0$ as well as for non-vanishing magnetic field (i.e. increasing K). In addition, an increase of B results in a decreasing cross section, again as in $p-H$ collisions. Due to the irregular motion of the positronium(cf. Fig. 4.1), the velocity matching effect is not expected

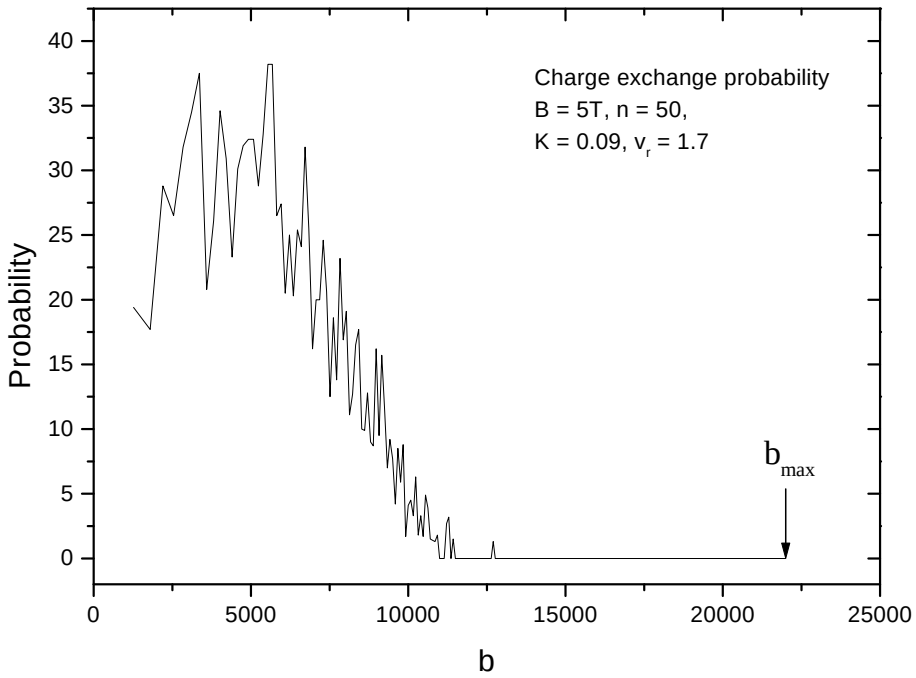

Figure 4.5: Impact-parameter dependent charge exchange probability. Impact velocity $v_r = 1.7$, external magnetic field $B = 5T$, $n = 50$, $K = 0.09$.

to play an important role. Thomas capture [12, 13], that happens in the collision plane in the field-free case [15], is foiled due to the magnetic field.

The observed behavior will be of interest for future experiments of the type $\bar{p} - e^+e^-$ or $\bar{p} - 2e^+$ collisions. Evidently, the magnetic field reduces the cross section, but this reduction remains within reasonable limits. Further explorations in the parameter space of cross section changes with K and binding energy would be worthwhile.

Chapter 5

Conclusions

In this thesis, the CTMC method is first applied to study the collisions between multiply charged ions and oriented elliptical Rydberg atoms at intermediate velocities. An extended CTMC equipped with a new method for generating a stationary microcanonical ensemble for a quasi-integrable one-body initial-state Hamiltonian is then used for multiply charged ion-Rydberg atom collisions in an external magnetic field. Finally, a modified CTMC method, which treats a two-body initial state system in a magnetic field, is constructed to investigate the behavior of antiproton and positronium collisions in an external magnetic field.

In the collisions between multiply charged ions and oriented elliptical Rydberg atoms, the roles of the spatial and the momentum distributions of the target electron states are illuminated in classical terms. The velocity matching phenomenon and Thomas effect in the upstream-downstream asymmetry are observed in the collisions, resulting in relatively larger charge exchange cross-section. Obviously, these effects are due to the involvement of the different spatial distributions. At the same time, the increasing projectile charge weakens the influence of the initial electron momentum distribution in the collisions. The important role of the initial electron

momentum distribution found for singly charged ion impact is strongly diminished for higher projectile charge. The reason is that, for increasing projectile charge, the distortion of the initial states caused by the strong perturbation of approaching ion induces pronounced changes in the momentum distribution. However, the initial spatial orientation of the electron remains an important role for all charge values under consideration. We must indicate that the results of increasing projectile charge illuminates an inherent weakness of the CTMC-approach: the slow rise of the electric field may "in reality" induce adiabatic transitions between the many Rydberg states which would be populated differently in the classical calculation.

In the collisions between singly and multiply charged ions and the hydrogen Rydberg atoms in a magnetic field of up to 4T, the magnetic field as well as projectile charge show us their influences on the charge exchange cross sections. For the target atoms with $n = 28$ and the magnetic quantum number $m = 2$, the ratio of magnetic energy to target atom Coulomb energy is of the order 0.1, therefore n and m are still good quantum numbers, but the electron angular momentum l is not. The target atom is in the l-mixing regime. The electronic states are characterized by a new quantum number k. The state with minimum k value (k_{min} state) corresponds to the higher set of energy and the state with maximum k value (k_{max} state) corresponds to the lower set of energy. First of all, a cross section reduction in case of an increasing magnetic field is found for multiply charged projectiles, which coincides with the results for singly charged ion impact. The structure effect due to the change of the initial state distribution by the magnetic field is effective in the collisions, resulting in different capture cross sections in k_{max} and k_{min} states. The strong z-momentum components in the cigar-shaped k_{max}-state facilitate capture at higher impact velocities, causing a

significant shift of k_{max} cross section. Secondly, for increasing projectile charge, empirical scaling quantities (σ/Q^{α} and $v_r/Q^{1/4}$) are found for the charge exchange cross sections, with $\alpha = 1$ for k_{max} and $\alpha = 1.2$ for k_{min} states. Higher projectile charges strongly enhance the charge exchange cross sections. However compared to singly charge projectile $Q = 1$, the contributions of various swaps spread over wider velocity increments and for increasing projectile charge the swap structure found in singly charge impact is washed out. This may be interpreted by the general phenomenon which also appears in our orientation studies with highly charged ions. That is: the strong long-range Coulomb attraction increasingly dominates over the influence of different target electron distributions.

The further exploration of collisions between antiprotons and Rydberg positroniums in a magnetic field gives us a deeper understanding of the influence of an external magnetic field on such collisions and also provides an alternative route for the antihydrogen formation. The initial state of a special case of a two-body system, positronium in a magnetic field, has been constructed by means of a newly introduced operator, the pseudomomentum $\mathbf{K}$. This value is the key to this problem for solving the non-separation which arises due to the finite nuclear masses of the system. It represents a conserved quantity, making it possible for a neutral system to perform a pseudoseparation of the center-of-mass motion. The initial Rydberg positronium in the states $n = 40$ and 50 for the magnetic field strengths of 4T and 5T have been investigated and compared to two field-free cases, namely, with angular momenta $l = n - 1 = m$ and $l = n - 1, m = 0$ (i.e., for circular Rydberg motion in planes perpendicular and parallel to the z direction, respectively). In the presence of the

magnetic field, the positronium is stable and delocalized. However the spatial distribution of positronium has changed to an irregular motion, leading to the probability for positron-electron overlap remaining near zero. It results in a cross section reduction of a magnitude similar to the one observed in $p-H$ collisions [29]. In addition, a smaller positronium binding energy (increasing n) and a larger geometrical extension of the target positronium atom (increasing K) yield a larger capture cross section. An increase of the magnetic field strength results in a decreasing cross section, again as in $p-H$ collisions. Due to the irregular motion of the positronium the velocity matching effect does not play an important role. Thomas capture which happens in the collision plane in the field-free case is foiled. The observed behavior may be of interest for future experiments of the type $\bar{p}-e^+e^-$ or $\bar{p}-2e^+$ collisions.

In this work, the CTMC method has been successfully carried out to solve the problem of multiply charged ion-Rydberg atom collisions with and without the presence of the magnetic field. The resulting CTMC cross sections are worthwhile to guide the analysis of the experimental data. Furthermore, using the extended CTMC method, it should be possible to study ion-Rydberg atom collision in very high magnetic fields, up to the Landau regime. Further explorations in the parameter space of cross section changing with pseudomomentum K, magnetic field B and the binding energy will be interesting subjects.

Bibliography

[1] R. F. Stebbings. *Sci.*, **193**, 537, 1976.

[2] T. F. Gallagher, L. M. Humphre, W. E. Cooke, R. M. Hill, and S. A. Edelstein. *Phys. Rev. A*, **16**, 1098, 1977.

[3] T. H. Jeys, G. W. Foltz, K. A. Smith, E. J. Beiting, F. G. Kellert, F. B. Dunning, and R. F. Stebbings. *Phys. Rev. Lett.*, **44**, 390, 1980.

[4] K. B. MacAdam and R. G. Rolfes. *J. Phys. B: At. Mol. Phys.*, **15**, L243, 1982.

[5] S. B. Hansen, G. Gray, E. Horsdal-Pedersen, and K. B. MacAdam. *J. Phys. B*, **24**, L315, 1991.

[6] Th. Wörmann, Z. Roller-Lutz, and H. O. Lutz. *Phys. Rev. A*, **47**, R1594, 1993.

[7] S. B. Hansen, T. Ehrenreich, E. Horsdal-Pedersen, K. B. MacAdam, and L. J. Dubé. *Phys. Rev. Lett.*, **71**, 1522, 1993.

[8] T. Ehrenreich, J. C. Day, S. B. Hansen, E. Horsdal-Pedersen, K. B. MacAdam, and K. S. Mogensen. *J. Phys. B*, **27**, L383, 1994.

[9] K. B. McAdam, J. C. Day, J. C. Aguilar, D. M. Homan, A. D. MacKellar, and N. J. Cavagnero. *Phys. Rev. Lett.*, **75**, 1723, 1995.

[10] O. P. Sorokina, D. M. Homan, O. P. Makarov, and K. B. MacAdam. *Bull. Am. Phys. Soc.*, **42**, 10333, 1997.

[11] J. C. Day, B. D. Depaola, T. Ehrenreich, S. B. Hansen, E. Horsdal-Pedersen, Y. Leontiev, and K. S. Mogensen. *Phys. Rev. A*, **56**, 4700, 1997.

[12] L. H. Thomas. *Proc. R. Soc. London, Ser. A*, **114**, 561, 1927.

[13] R. Shakeshaft and L. Spruch. *Rev. Mod. Phys.*, **51**, 369, 1979.

[14] S. Bradenbrink, H. Reihl, Th. Wörmann, Z. Roller-Lutz, and H. O. Lutz. *J. Phys. B: At. Mol. Opt. Phys.*, **27**, L391–L394, 1994.

[15] S. Bradenbrink, H. Reihl, Z. Roller-Lutz, and H. O. Lutz. *J. Phys. B: At. Mol. Opt. Phys.*, **28**, L133–L138, 1995.

[16] R. E. Olson. *J. Phys. B: At. Mol. Opt. Phys.*, **13**, 483, 1980.

[17] R. Abrines and I. C. Percival. *Proc. Phys. Soc.*, **88**, 861, 1966.

[18] R. E. Olson and A. Salop. *Phys. Rev. A*, **16**, 531–541, 1977.

[19] J. Pascale, R.E. Olson, and C. O. Reinhold. *Phys. Rev. A*, **42**, 5305, 1990.

[20] I. Fourré and C. Courbin. *Z. Phys. D*, **38**, 103–111, 1996.

[21] D. M. Homan, O. P. Makarov, O. P. Sorokina, K. B. MacAdam, M. F. V. Lundsgaard, C. D. Lin, and N. Toshima. *Phys. Rev. A*, **58**, 4565, 1998.

[22] L. Kristensen, T. Bové, B. D. Depaola, T. Ehrenreich, E. Horsdal-Pedersen, and O. E. Povlsen. *J. Phys. B*, **33**, 1103, 2000.

[23] S. Suzuki, N. Shimakura, and M. Kimura. *J. Phys. B*, **29**, 1063, 1996.

[24] S. Bivona and M. R. C. McDowell. *J. Phys. B*, **20**, 1541, 1987.

[25] U. Wille. *Phys. Rev. Lett. A*, **125**, 52, 1987.

[26] T. P. Grosdanov and M. R. C. McDowell. *J. Phys. B*, **18**, 921, 1985.

[27] H. Ruder, G. Wunner, H. Herold, and F. Geyer. *Atoms in Strong Magnetic Fields*. Springer-Verlag, Berlin, 1984.

[28] S. Bradenbrink, E. Y. Sidky, Z. Roller-Lutz, H. Reihl, and H. O. Lutz. *J. Phys. B: At. Mol. Opt. Phys.*, **30**, L161–L166, 1997.

[29] S. Bradenbrink, E. Y. Sidky, Z. Roller-Lutz, H. Reihl, and H. O. Lutz. *Phys. Rev. A*, **55**, 4290, 1997.

[30] S. Bradenbrink, H. Reihl, Z. Roller-Lutz, and H. O. Lutz. *J. Phys. B: At. Mol. Opt. Phys.*, **30**, 1–13, 1997.

[31] J. Shertzer, J. Ackermann, and P. Schmelcher. *Phys. Rev. A*, **58**, 1129, 1998.

[32] J. Lu, S. Bradenbrink, Z. Roller-Lutz, and H. O. Lutz. *J. Phys. B: At. Mol. Opt. Phys.*, **32**, L681–L686, 1999. J. Phys. B: At. Mol. Opt. Phys. **33**:2947, 2000.

[33] J. E. Avron, I. W. Herbst, and B. Simon. *Ann.Phys. (N.Y.)*, **114**, 431, 1978.

[34] H. Herold, H. Ruder, and G. Wunner. *J. Phys. B*, **14**, 751, 1981.

[35] G. Wunner, H. Ruder, and H. Herold. *Phys. Lett.*, **79A**, 159, 1980.

[36] B. R. Johnson, J. Hirschfelder, and Kuo-Ho. Yang. *Rev. Mod. Phys.*, **55**, 109, 1983.

[37] P. Schmelcher, L. S. Cederbaum, and H. D. Meyer. *Phys. Rev. A*, **38**, 6066, 1988. J. Phys. B, **21**:L445, 1988.

[38] M. Vincke and D. Baye. *J. Phys. B*, **21**, 2407, 1988.

[39] D. Baye and M. Vincke. *J. Phys. B*, **23**, 2467, 1990.

[40] P. Schmelcher and L. S. Cederbaum. *Phys. Rev. A*, **43**, 287, 1991.

[41] P. Schmelcher and L. S. Cederbaum. *Z. Physik* ***D***, **24**, 311, 1992.

[42] P. Schmelcher and L. S. Cederbaum. *Chem. Phys. Lett.*, **208**, 548, 1993.

[43] J. S. Cohen. *Phys. Rev. A*, **26**, 3008–3010, 1982.

[44] D. Banks, R. S. Barnes, and J. Wilson. *J. Phys. B*, **9**, 141, 1976.

[45] R. L. Becker and A. D. Mackellar. *J. Phys. B*, **17**, 3923, 1984.

[46] G. Peach, S. L. Willis, and M. R. C. McDowell. *J. Phys. B: At. Mol.*, **18**, 3921–3937, 1985.

[47] C. O. Reinhold and C. A. Falcon. *Phys. Rev. A*, **33**, 3859–3866, 1986.

[48] G. A. Kohring, A. E. Wetmore, and R. E. Olson. *Phys. Rev. A*, **28**, 2526–2528, 1983.

[49] R.E.Olson, J. Wang, and J. Ullrich. In *Electronic and Atomic Collisions, eds. H.B. Gilbody, W.R. Newell, F.H. Read, A.C.H. Smith*, page 271. North Holland, 1987. AIP Conf. Proc. **295**, 520, 1993.

[50] U. Fano, F. Robicheaux, and A. R. P. Rau. *Phys. Rev. A*, **37**, 3655, 1988.

[51] P. A. Braun. *Zh. Eksp. Teor. Fiz.*, **84**, 850, 1983. [Sov. Phys. JETP **57**, 492 (1983)].

[52] E. A. Solov'ev. *Sov. Phys. -JETP*, **55**, 1017, 1982.

[53] R.K. Janev, L.P. Presnyakov, and V.P. Shevelko. *Physics of Highly Charged Ions.* Springer Series in Electrophysics 13, 1985.

[54] V.P. Shevelko. *Atoms and Their Spectroscopic Properties.* Springer Series on Atoms and Plasmas 18, 1997.

[55] G. Gabrielse, D. S. Hall, T. Roach, P. Yesley, A. Khabbaz, J. Estrada, C. Heimann, and H. Kalinowsky. *Phys, Lett. B*, **455**, 311–315, 1999.

[56] J. Estrada, T. Roach, J. N. Tan, P. Yesley, and G. Gabrielse. *Phys. Rev. Lett.*, **84**(5), 859, 2000.

[57] G. Gabrielse, N. S. Bowden, P. Oxley, A. Speck, C. H. Storry, J. N. Tan, M. Wessels, D. Grzonka, W. Oelert, G. Schepers, T. Sefzick, J. Walz, H. Pittner, T. W. Hänsch, and E. A. Hessels. *Phys. Rev. Lett.*, **89**(21), 213401, 2002.

[58] G. Gabrielse, N. S. Bowden, P. Oxley, A. Speck, C. H. Storry, J. N. Tan, M. Wessels, D. Grzonka, W. Oelert, G. Schepers, T. Sefzick, J. Walz, H. Pittner, T. W. Hänsch, and E. A. Hessels. *Phys.Rev. Lett.*, **89**(23), 213401, 2002.

[59] M. Amoretti et al. *Nature (London)*, **419**, 456, 2002.

[60] D. B. Cassidy, J. P. Merrison, M. Charlton, J. Mitray, and G. Ryzhikh. *J. Phys. B: At. Mol. Opt. Phys.*, **32**, 1923, 1999.

[61] J. S. Briggs and E. A. Solovév. *J. Phys. B: At. Mol. Opt. Phys.*, **34**, 1337, 2001.

[62] P. Schmelcher. *J. Phys.* ***B***, **25**, 2697, 1992.

[63] O. Dippel, P. Schmelcher, and L. S. Cederbaum. *Phys. Rev. A*, **49**, 4415, 1994.

[64] J. Shertzer, J. Ackermann, and P. Schmelcher. *Phys. Rev. A*, **58**, 1129, 1988.

Appendix A

Published and submitted papers

A.1 Classical trajectory Monte Carlo calculations of electron capture and ionization in collisions of multiply charged ions with elliptical Rydberg atoms

RAPID COMMUNICATIONS

PHYSICAL REVIEW A, VOLUME 62, 050701(R)

Classical trajectory Monte Carlo calculations of electron capture and ionization in collisions of multiply charged ions with elliptical Rydberg atoms

J. Lu,[1] Z. Roller-Lutz,[2] and H. O. Lutz[1]
[1]*Fakultät für Physik, Universität Bielefeld, 33501 Bielefeld, Germany*
[2]*Institute of Physics, Faculty of Medicine, Rijeka University, HR-5100 Rijeka, Croatia*
(Received 11 April 2000; published 11 October 2000)

We have performed classical trajectory Monte Carlo studies of electron capture and ionization in multiply charged ($Q \leqslant 8$) ion–Rydberg-atom collisions at intermediate impact velocities. Impact parallel to the minor and to the major axis, respectively, of the initial Kepler electron ellipse has been investigated. The important role of the initial electron momentum distribution found for singly charged ion impact is strongly diminished for higher projectile charge, while the initial spatial distribution remains important for all values of Q studied.

PACS number(s): 34.60.+z, 34.70.+e

The use of coherent elliptical Rydberg states in ion-atom collision studies (for recent papers on the subject cf. [1–3] and references therein) has not only aided the intuitive understanding of the interaction dynamics, it also illuminates the roles of the momentum and the spatial distributions of the target electron states. In classical terms, the *momentum distribution* can be widely varied simply by changing the eccentricity ε of the Rydberg ellipse without affecting the energy of the state. In particular, for impact perpendicular to the major axis of the ellipse, the capture cross section displays a maximum if $\mathbf{v_p}$ (the perihelion electron velocity) is parallel and equal to the projectile velocity $\mathbf{v}$; this is believed to be due to the matching electron momenta in the initial target and the final projectile state. In contrast, the role of the *spatial distribution* becomes most clearly visible if the impact velocity vector is adjusted perpendicular to the minor axis of the Rydberg ellipse; in this case, the electrons can be located either between the approaching ion and the target nucleus (''upstream geometry'') or behind the target nucleus, as seen from the projectile (''downstream geometry'') without otherwise changing the momentum distribution of the Rydberg state (i.e., its angular momentum l and the principal quantum number n). The capture cross section in both cases turns out to be quite different: it is much larger in the upstream case as compared to the downstream case; apparently, in the corresponding region of parameter space the spatial characteristics of the initial state determine the outcome of the collision. These investigations have so far been restricted to collisions with singly charged ions. Recently, however, it has become possible to employ such targets in studies involving multiply charged ions [1,4]. In another context (electron capture by multiply charged ions in the presence of an external magnetic field) we have found indications [5] that for increasing projectile charge Q the distortion of the initial state increasingly dominates the influence of different target electron distributions. We have therefore performed an exploratory study of such systems in which a spatially oriented Rydberg atom collides with a multiply charged ion. This is the topic of this paper.

We employ the classical trajectory Monte Carlo (CTMC) method, which is quite useful in particular for the description of quantum-mechanically complex systems, giving a good qualitative and often fairly quantitative agreement with experimental data (for more recent applications to the study of Rydberg atom collisions cf., e.g., [1–3]). Structureless ions of charge Q between 1 and 8 collide with Rydberg target atoms with nuclear charge $q=1$ and principal quantum number $n=25$. The geometry is chosen such that the direction of impact is perpendicular to the angular-momentum direction of the Kepler ellipse. Specifically, two cases are studied: (i) impact is parallel to the minor axis, thus allowing one to study the velocity matching phenomenon, and (ii) impact parallel to the major axis, showing the effect of the spatial orientation of the target electron (''upstream-downstream asymmetry''). A useful quantity characterizing the electron orbit is the (generalized) eccentricity $\varepsilon = \pm\sqrt{1-(l/n)^2}$. In case (i), the + (−) sign identifies orbits with the perihelion velocity $\mathbf{v_p}$ parallel (antiparallel) to $\mathbf{v}$; in case (ii) it characterizes the upstream (downstream) geometry. The impact velocity v is scaled by $1/n$, the velocity of a circular Rydberg state, i.e., $V=vn=1$ in this case; the number of MC cycles was adjusted to obtain statistical uncertainties of less than 5%. Care has been taken to assure that the projectile starts

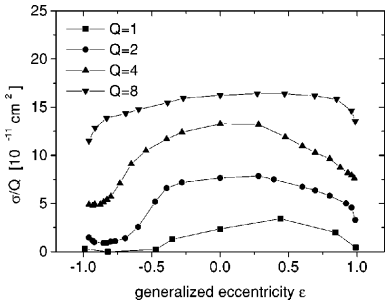

FIG. 1. Eccentricity-dependent capture cross section σ/Q for impact velocity $V=1.66$ (in units of the circular $n=25$ Rydberg electron velocity) and different projectile charges Q. Impact is parallel to the minor axis. For the initial state, velocity matching is obtained at $\varepsilon=+0.47$.

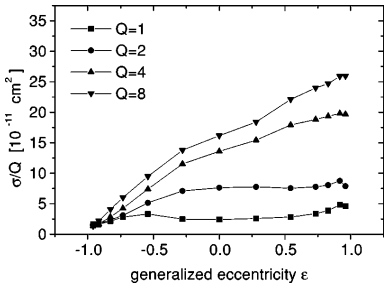

FIG. 2. Eccentricity-dependent capture cross section σ/Q for impact velocity $V=1.66$ and different projectile charges Q. Impact is parallel to the major axis; $\varepsilon>0$ (<0) corresponds to the upstream (downstream) geometry.

sufficiently far from the target [approximately 3.5×10^5 atomic units (a.u.)] to correctly describe the initial part of the trajectory; in view of the long-range Coulomb potential and the known sensitivity of Rydberg states to l,m changing processes, this is critical particularly for higher projectile charges Q (see also below).

(i) Impact parallel to the minor axis. Figure 1 shows the eccentricity-dependent charge-capture cross section σ/Q for $V=1.66$ and Q ranging from 1 to 8. Velocity matching is obtained at $\varepsilon=+0.47$; at low Q, the cross section displays the well-known behavior with a pronounced maximum at this eccentricity and a deep minimum for negative eccentricities that characterize a strongly elongated Kepler ellipse with **v** antiparallel to $\mathbf{v_p}$. For increasing Q, this structure is soon washed out; while it is still noticeable for $Q=2$ and 4, almost any trace of the minimum has disappeared for $Q=8$. Inspection of electron trajectories during the approach of the projectile ion reveals the reason: as expected, the long-range Coulomb force distorts the original Kepler ellipse already at quite long distances. This distortion is quite regular, and reminds one of a Stark effect. Indeed, a simple estimate confirms this: for $Q=8$, an electric-field strength of 5 V/cm (i.e., of the order of the fields applied to the collision region in the experiments [1]) is attained at approximately 10^5 a.u. This initial-state effect might be reduced in the experiment by applying a strong field in the target region; however, this result also illuminates an inherent weakness of the CTMC approach: the slow rise of the electric field may ''in reality'' induce adiabatic transitions between the many Rydberg states that would be populated differently in the classical calculation. This distortion of the initial state becomes quite severe at distances below 10^4 a.u., i.e., corresponding to several revolutions of the Rydberg electron about its nucleus; therefore, it is to be believed that the washing out of the cross-section structure is indeed a real effect. Finally, we may add that also the impact-parameter dependence of the capture probability reflects the signature of this effect. While for $Q=1$ and $\varepsilon=+0.47$ (the velocity-matching situation) the capture probability is rather concentrated about the peri-

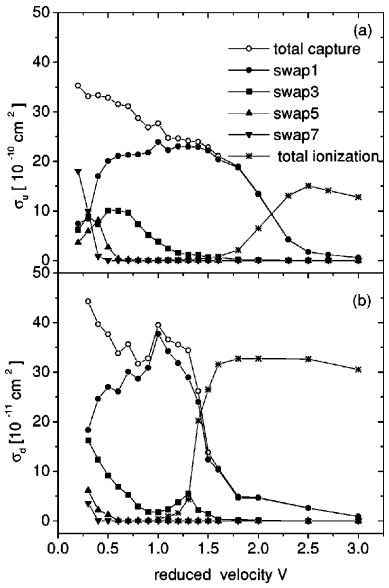

FIG. 3. Charge-capture cross sections ($Q=8$) for (a) upstream σ_u and (b) downstream σ_d geometry; the eccentricity $\varepsilon=\pm0.96$. The respective ionization cross sections are also given.

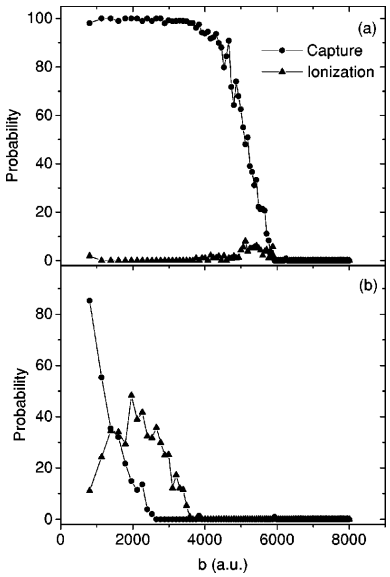

FIG. 4. Impact-parameter-dependent probabilities of capture and ionization: (a) upstream geometry, (b) downstream geometry. Impact parameter b in atomic units; impact velocity $V=1.5$; projectile charge $Q=8$.

helion position [6], it is nearly symmetric about $b=0$ (the position of the target nucleus) for $Q=8$.

(ii) Impact parallel to the major axis. Figure 2 shows the eccentricity-dependent charge-capture cross section σ/Q for $V=1.66$. As in the case of singly charged projectiles $Q=1$ [2], the cross section for multiply charged ions ($Q=2$, 4, and 8) is much higher for the upstream geometry as compared to the downstream geometry. For a more detailed study we choose $\varepsilon=\pm 0.96$, corresponding to $l=7$. This creates quite elongated states that are not too nonclassical (low l). Figure 3 shows for $Q=8$ the cross sections for upstream (σ_u) and downstream (σ_d) geometry, respectively, including the contributions of the various ''swaps'' to the capture cross sections. A swap has been defined as a passage of the electron through the midplane between projectile and the target nucleus [7]; note, however, that for asymmetric collisions ($q \neq Q$ as studied here), this plane has to cut the connection line between target and projectile nucleus at the saddle point of the two respective Coulomb potentials [i.e, at a distance $R/(1+\sqrt{q/Q})$ from the projectile, with R the distance of both nuclei]. In view of the discussion in case (i) above, the strong upstream-downstream asymmetry seen in these data is at first glance somewhat surprising. Again, inspection of the electron trajectories sheds light on this point: the slowly increasing electric field of the approaching projectile causes a distortion and precession of the Kepler ellipse, in general not strong enough, however, to revert the upstream into a downstream geometry and *vice versa*. Therefore, upon the approach of the projectile into the actual close interaction the electron is still mainly fore or aft, respectively, of the target nucleus, thus qualitatively preserving the role of the initial spatial distribution of the electron; interestingly, even three-swap and higher-swap processes can still be discerned. The qualitatively different behavior of σ_u and σ_d beyond $V=1.5$ is associated with differently rising cross sections for ionization; in case of the downstream geometry it sets in at considerably smaller V values as compared to the upstream geometry. This is further clarified by the respective impact-parameter dependencies [Figs. 4(a) and (b)]: In the upstream situation, charge-exchange extends out to fairly large distances and ionization is still weak; in the downstream situation, the maximum charge exchange probability is of the same order as in the upstream case; however, it is limited to much smaller impact parameters, and ionization is already quite strong.

To conclude, our analysis shows that for impact of multiply charged ions of intermediate velocities the role of the initial electron momentum distribution becomes weaker for increasing projectile charge. This is due to the strong perturbation of the initial state by the approaching ion that induces pronounced changes in the momentum distribution long before the actual close interaction occurs. In contrast, the initial spatial orientation of the electron continues to be important for all Q values studied here.

This work has been supported by the Deutsche Forschungsgemeinschaft (DFG).

[1] J. C. Day, B. D. DePaola, T. Ehrenreich, S. B. Hansen, E. Horsdal-Pedersen, Y. Leontiev, and K. S. Mogensen, Phys. Rev. A **56**, 4700 (1997).

[2] D. M. Homan, O. P. Makarov, O. P. Sorokina, K. B. MacAdam, M. F. V. Lundsgaard, C. D. Lin, and N. Toshima, Phys. Rev. A **58**, 4565 (1998).

[3] L. Kristensen, T. Bové, B. D. DePaola, T. Ehrenreich, E. Horsdal-Pedersen, and O. E. Povlsen, J. Phys. B **33**, 1103 (2000).

[4] B. D. DePaola (private communication).

[5] J. Lu, S. Bradenbrink, Z. Roller-Lutz, and H.O. Lutz, J. Phys. B **32**, L681 (1999); **33**, 2947 (2000).

[6] S. Bradenbrink, H. Reihl, Z. Roller-Lutz, and H.O. Lutz, J. Phys. B **28**, L133 (1995).

[7] K. B. MacAdam, J. C. Day, J. C. Aguilar, D. M. Homan, A. D. MacKellar, and N. J. Cavagnero, Phys. Rev. Lett. **75**, 1723 (1995).

A.2 Electron capture in multiply charged ion-Rydberg atom collisions in an external magnetic field

J. Phys. B: At. Mol. Opt. Phys. **32** (1999) L681–L686. Printed in the UK PII: S0953-4075(99)07204-1

LETTER TO THE EDITOR

Electron capture in multiply charged ion–Rydberg atom collisions in an external magnetic field

J Lu, S Bradenbrink, Z Roller-Lutz† and H O Lutz

Fakultät für Physik, Universität Bielefeld, 33501 Bielefeld, Germany

E-mail: lutz@physik.uni-bielefeld.de

Received 25 August 1999

Abstract. Using the classical trajectory Monte Carlo method, we calculated charge transfer cross sections for 1.27–183 eV amu^{-1} singly and multiply charged ions ($Q = 1, 2, 4$ and 8) colliding with Rydberg atoms in a magnetic field of up to 4 T. The results show a significant influence of the magnetic field, and the velocity-dependent cross sections become increasingly featureless for increasing projectile charge.

In recent papers [1–3] we have studied ionization and charge capture for singly charged ion–Rydberg atom collisions in external magnetic fields; such systems are of interest for astrophysics as well as plasma physics. In these studies, the field strength was chosen such that the magnetic energy of the active electron is comparable to the Coulomb energy in the field of the target nucleus; in addition, we have restricted ourselves to experimentally accessible fields of up to a few tesla. Both requirements can be met if the target atoms are in Rydberg states with high principal quantum numbers n. In our work, we chose $n = 28$ and the magnetic quantum number $m = 2$; these states can easily be prepared by laser-optical pumping. Such collision systems are at the boundary of classical and quantum mechanics. Since they are not yet accessible to a quantum mechanical treatment, we apply the classical trajectory Monte Carlo (CTMC) method. For ion–atom collisions, this method has been made popular by the work of Olson and co-workers (cf, e.g., [4]), and is known to be quite useful, in particular, for quantum mechanically complex systems (such as, for example, Rydberg atom collisions). With the ratio of magnetic energy to target atom Coulomb energy of the order 0.1, n and m are still good quantum numbers, but the electron angular momentum l is not. Under these conditions, the electronic states are characterized by a new quantum number k, with its minimum value $k_{\min} = 0$ corresponding to a disc-shaped state (somewhat similar to the field-free $l = m = 2$ state), and the $k_{\max} = 24$ state is elongated along the magnetic field (z-)axis ('cigar shape'). We assume that the projectile ion moves at a constant velocity parallel to the magnetic field, and the target nucleus remains motionless; due to the spatial extension of the electron state and the corresponding large impact parameters, this is a good approximation. The Hamiltonian governing the electron trajectory is

$$H = p^2/2 - 1/\vec{r} - 1/|\vec{r} - \vec{R}| + \gamma l_z/2 + \gamma^2\rho^2/8$$

† Present address: Institute of Physics, Faculty of Medicine, Rijeka University, Rijeka, Croatia.

0953-4075/99/240681+06$30.00

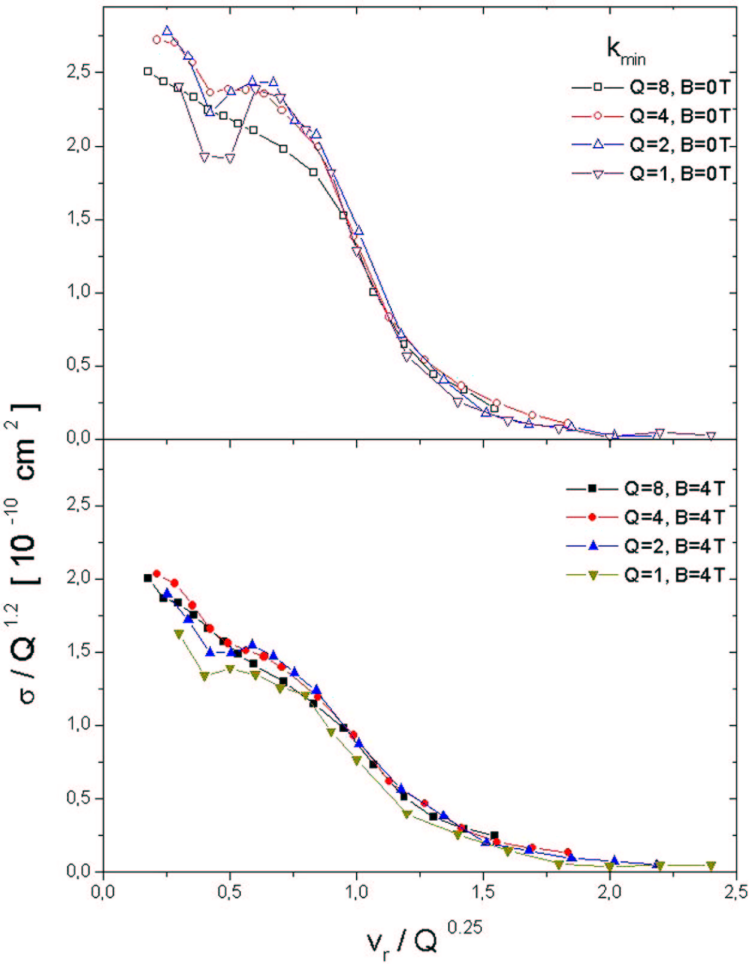

Figure 1. Velocity-dependent charge exchange cross section for collisions of Q-fold ionized projectiles with targets in the $k_{\min}$ initial state. Top, field-free condition ($B = 0$); bottom, external magnetic field $B = 4$ T.

where $\vec{R} = \vec{b}+\vec{v}t$; $\gamma = B/(2.3505\times10^5\ \mathrm{T})$; $\rho^2 = x^2+y^2$. l_z is the z-component of the electron angular momentum; B is the magnetic field strength expressed in tesla; $\vec{R}$ is the internuclear vector, $\vec{b}$ the impact parameter and $\vec{v}$ the ion velocity in the target frame chosen parallel to the magnetic field.

In this letter, we extend our calculations from singly charged ion impact ($Q = 1$) to ion charges $Q = 2, 4$ and 8 at magnetic field strengths of 0, 2 and 4 T. The collision energies (between 1.27 and 183 eV amu^{-1}) correspond to impact velocities v_r between 0.2 and 2.4 ($v_\mathrm{r} = v/v_\mathrm{e}$, with v_e the classical electron velocity in a circular $n = 28$ orbit).

The resulting velocity-dependent charge exchange cross sections for $k_{\max}$ and $k_{\min}$ states are shown in figures 1 and 2. Two effects can be seen: (a) an external magnetic field reduces the

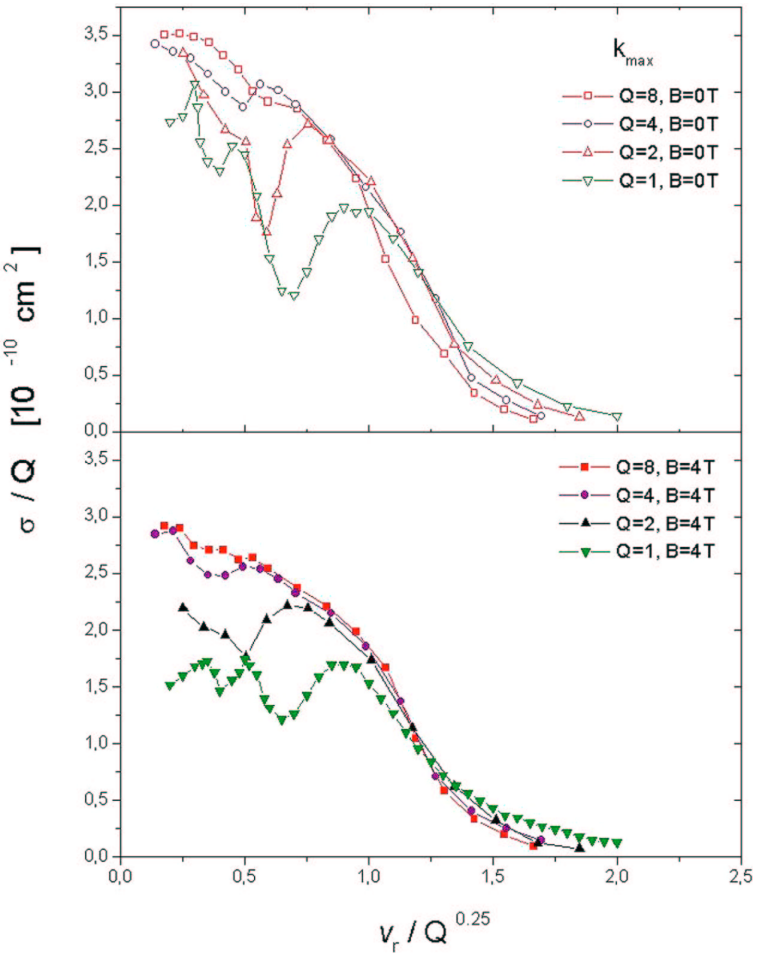

Figure 2. As in figure 1, but the target is in the k_{max} initial state.

cross sections and (b) an increase of the projectile charge washes out the structures observed in the $Q = 1$ cross sections.

B dependence

The cross section reduction in the case of an increasing magnetic field has already been found for singly charged projectiles [2]. We may recall that the influence of the field is twofold; it alters the initial electron state distribution ('structure effect') as well as the charge exchange dynamics. The structure effect can be separated by looking at the difference between the k_{max} and the k_{min} cross sections for $B = 0$. It contains the influence of the initial state momentum distribution (i.e. the effect of the matching velocities of the projectile and the captured electron) as well as their spatial extension. Although the structure effect

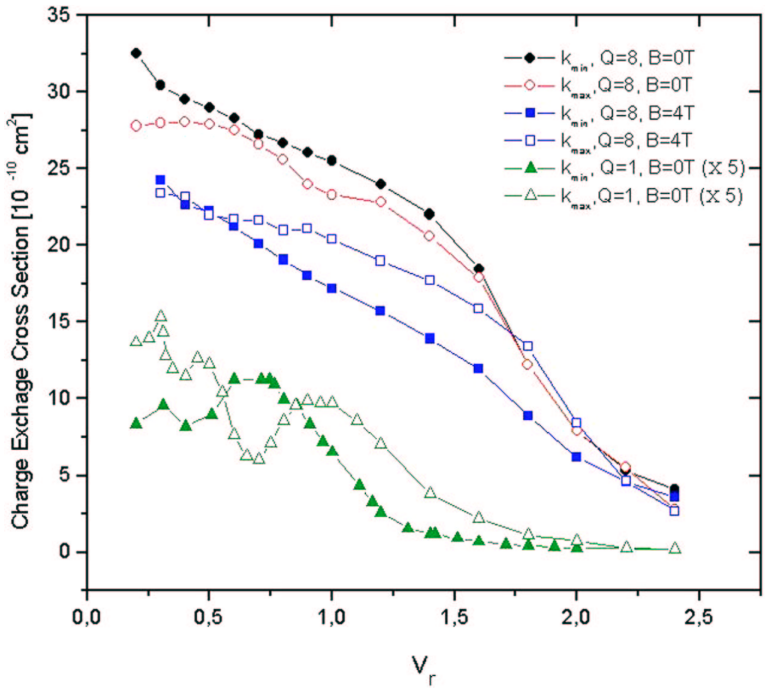

Figure 3. Comparison of $k_{\min}$ and $k_{\max}$ cross sections for different projectile charge and magnetic field.

appears to be somewhat reduced for increasing Q (cf the $B = 0$ curves in figure 3), at $B = 4$ T the $k_{\max}$ cross section is still significantly shifted to higher v_r compared to the $k_{\min}$ cross section; this shift has been interpreted as a signature of the velocity matching effect [2]. The strong z-momentum components in the cigar-shaped $k_{\max}$-state facilitate capture at higher impact velocities. The $Q = 2$ and 4 projectiles yield a behaviour between $Q = 1$ and 8.

Q dependence

Following [5], we have chosen in figures 1 and 2 σ/Q^{α} and $v_r/Q^{1/4}$ as scaling quantities; for the $k_{\max}$ initial state $\alpha \approx 1$, while $\alpha \approx 1.2$ gives a somewhat better fit in the case of $k_{\min}$.

Particularly pronounced deviations from the simple scaling in figures 1 and 2 show up at $v_r < 1$. The cross section structure at these velocities has been attributed to the so-called 'swaps' [2, 6, 7], i.e. the repeated passage of the electron through the projectile–target midplane. The order of swaps characterizes how often the electron passes through the midplane before it finally stays with the projectile. As an example, figure 4 displays the contributions of the various swaps to the $k_{\min}$-charge exchange cross section when the projectile is singly ($Q = 1$) or highly charged ($Q = 8$); $k_{\max}$ behaves qualitatively similar. Compared to $Q = 1$ the contributions of the various swaps spread over wider velocity increments, and the swap structure is washed out. Evidently, for increasing Q, the strong long-range Coulomb attraction increasingly dominates

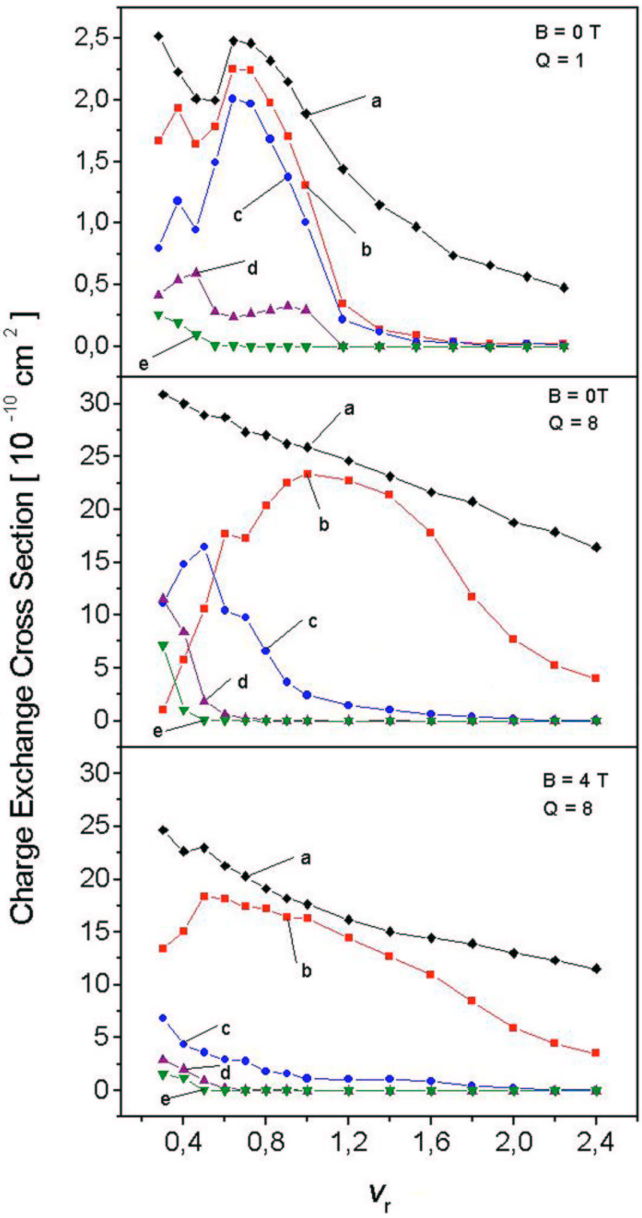

Figure 4. Contributions of 'swaps' to the total charge exchange cross section (a) for k_{min} initial target states: (b) one swap, (c) three swaps, (d) five swaps and (e) seven swaps.

over the influence of different target electron distributions. One may expect that this is a general phenomenon which should also be seen in other alignment/orientation studies with highly charged ions.

Discussions with J P Hansen and E Sidky are gratefully acknowledged. This work has been supported by the Deutsche Forschungsgemeinschaft (DFG).

References

[1] Bradenbrink S, Sidky E Y, Roller-Lutz Z, Reihl H and Lutz H O 1997 *J. Phys. B: At. Mol. Opt. Phys.* **30** L161
[2] Bradenbrink S, Sidky E Y, Roller-Lutz Z, Reihl H and Lutz H O 1997 *Phys. Rev.* A **55** 4290
[3] Bradenbrink S, Reihl H, Roller-Lutz Z and Lutz H O 1997 *J. Phys. B: At. Mol. Opt. Phys.* **30** 5819
[4] Olson R E 1987 *Electronic and Atomic Collisions* ed H B Gilbody, W R Newell, F H Read and A C H Smith (Amsterdam: North-Holland) p 271
Olson R E, Wang J and Ullrich J 1993 *AIP Conf. Proc.* **295** 520
[5] Janev R K, Presnyakov L P and Shevelko V P 1985 *Physics of Highly Charged Ions (Springer Series in Electrophysics vol 13)* (Berlin: Springer)
Shevelko V P 1997 *Atoms and Their Spectroscopic Properties (Springer Series on Atoms and Plasmas vol 18)* (Berlin: Springer)
[6] McAdam K B, Day J C, Aguilar J C, Homan D M, McKellar A D and Cavagnero N J 1995 *Phys. Rev. Lett.* **9** 1723
[7] Homan D M, Makarov O P, Sorokina O P, MacAdam K B, Lundsgaard M F V, Lin C D and Toshima N 1998 *Phys. Rev.* A **58** 4565

J. Phys. B: At. Mol. Opt. Phys. **33** (14 August 2000) 2947

CORRIGENDUM

Electron capture in multiply charged ion-Rydberg atom collisions in an external magnetic field

J Lu, S Bradenbrink, Z Roller-Lutz and H O Lutz
1999 *J. Phys. B: At. Mol. Opt. Phys.* **32** L681-L686

Figure 4 contains a misplotted total cross section curve. The correct figure 4 is shown below.

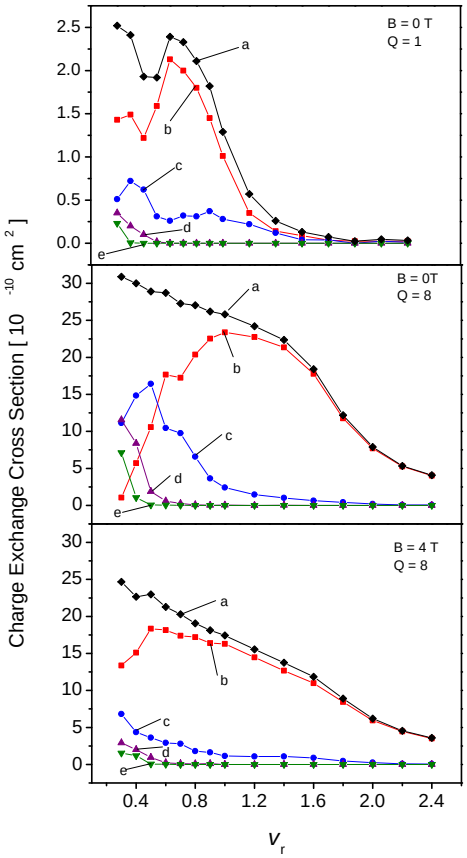

Figure 4. Contributions of 'swaps' to the total charge exchange cross section (a) for $k_{\min}$ initial target states, (b) one swap, (c) three swaps, (d) five swaps and (e) seven swaps.

A.3 Anti-hydrogen formation by collisions of anti-protons with positronium in a magnetic field (submitted to Phys. Rev. A)

Anti-hydrogen formation by collisions of anti-protons with positronium in a magnetic field

J. Lu[1], E.Y. Sidky[2], Z. Roller-Lutz[3], H. O. Lutz[1]
[1] *Fakultät für Physik, Universität Bielefeld, 33501 Bielefeld, Germany**
[2] *Department of Radiology, University of Chicago, 5841 S. Maryland Ave., Chicago, IL 60637, USA and*
[3] *Institute of Physics, Faculty of Medicine, Rijeka University, Rijeka, Croatia*

Using the classical trajectory Monte Carlo (CTMC) method, we calculated the charge transfer cross section for antiprotons ($\bar{p}$) colliding with Rydberg positronium (Ps), leading to antihydrogen formation. The results show a significant influence of an externally applied magnetic field which causes a reduction of the cross-section.

PACS numbers: 34.60.+z, 34.70.+e

The recent success of experiments to produce significant numbers of cold antihydrogen atoms has opened a new door to a test of fundamental symmetries in physics (cf. [1–3] and references therein). An accurate spectrometry of photon transitions in hydrogen and its antiparticle could resolve the question if the Rydberg constants in both systems are identical, as required by the CPT theorem. In these experiments slow antiprotons interact with positrons stored in a "nested trap" and capture processes yield cold antihydrogen atoms; three-particle $\bar{p}-2e^+$ recombination as well as radiative $\bar{p}-e^+$ recombination are discussed as possible causes for antihydrogen formation. However, as an alternative route also e^+ capture from positronium,

$$\bar{p} + (e^+e^-) \rightarrow \bar{H} + e^- \qquad (1)$$

has recently received considerable attention (cf. [4, 5] and references therein). For all these processes, a major problem in the quantitative interpretation lies in the unknown effect of the strong ($\approx$ 5 Tesla) magnetic field present in the trap. Therefore, in an extension of our previous CTMC calculations [6, 7] on $p-H$ collisional charge transfer and ionization in a magnetic field, we present some preliminary results for the latter problem(Eq. 1), namely, the effect of a strong magnetic field on $\bar{p}-Ps$ collisions. As suggested earlier [8], the positronium (Ps) target is assumed to be in a high Rydberg state. Thus, our study may also provide a first-step model to estimate the influence of the external magnetic field on the $\bar{p}-2e^+$ system. Both situations deal with a three-body collision involving two weakly interacting light particles, trapped at large distances from each other about their respective magnetic field lines.

The presence of a magnetic field in such calculations is by no means a trivial problem since in general the center-of-mass motion and the internal motion of the system cannot be separated. The first rigorous treatment of a two-body system in a magnetic field has been published by Avron, Herbst, and Simon [9]. A new operator connected with the center-of-mass motion, the so-called pseudomomentum $\mathbf{K}$, was introduced in their work. It represents a conserved quantity for the system, making it possible for neutral systems to perform a pseudoseparation of the center-of-mass motion. Later, a classical investigation of the highly excited hydrogen [10, 11] and positronium [12, 13] atoms in a magnetic field has been performed by P. Schmelcher, L.S. Cederbaum and coworkers. The Coulomb potential is distorted by the magnetic field, and above a critical value K_c of the pseudopotential an additional well forms on the negative x axis; it will be referred to as the outer well (OW). The outer well moves away from the magnetically distorted Coulomb potential and becomes broader and deeper with increasing K. Particles in this OW are trapped at large distances from each other, leading to delocalized states. Fig. 1 shows examples of this potential for Ps, the case of interest in this work.

As in our previous work on $p-H$ collisions in a magnetic field [6, 7] we applied the classical trajectory Monte Carlo (CTMC) method to calculate cross sections for the reaction (1). The target Ps atoms, embedded in magnetic fields of 4T and 5T, are in Rydberg states with binding energies corresponding to field-free principal quantum numbers $n = 40$ and 50. Unfortunately, in contrast to a Rydberg hydrogen atom with an "infinitely heavy" proton nucleus, the center-of-mass of Ps in a magnetic field is unstable. This makes a direct application of our CTMC method to the system under study here more difficult.

First we have to create the proper initial e^+e^- target states. To this end, we follow the treatment proposed by the Heidelberg group [12–14]. The nonrelativistic Hamiltonian of two particles with equal masses and opposite charges in a homogeneous static magnetic field is given by

$$H = \frac{1}{2}(\mathbf{p_1} + \mathbf{A_1})^2 + \frac{1}{2}(\mathbf{p_2} - \mathbf{A_2})^2 - \frac{1}{\mid \mathbf{r}_1 - \mathbf{r}_2 \mid} \qquad (2)$$

where $\mathbf{p_1}, \mathbf{p_2}$ and $\mathbf{r_1}, \mathbf{r_2}$ are the momenta and coordinates of the electron and positron, respectively. $\mathbf{A}_1 = \frac{1}{2}\mathbf{B}\times\mathbf{r_1}$, $\mathbf{A_2} = \frac{1}{2}\mathbf{B}\times\mathbf{r_2}$ are the symmetric gauge vector potentials

*Electronic address: lutz@physik.uni-bielefeld.de

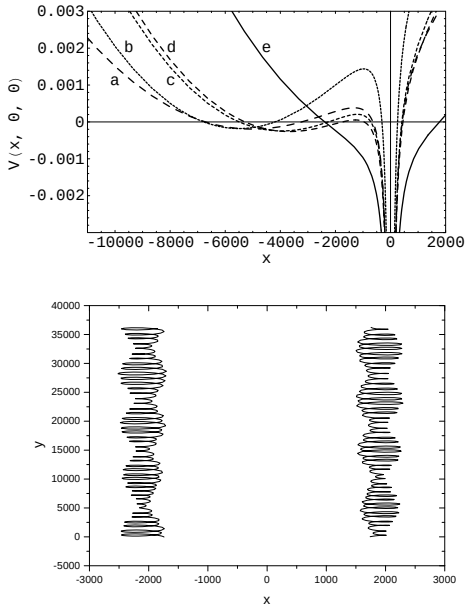

FIG. 1: Top: $V(x,0,0)$ for Ps in a magnetic field. a: $B = 4T, K = 0.09$, b: $B = 5T, K = 0.12$, c: $B = 5T, K = 0.09$, d: $B = 5T, K = 0.085$, e: $B = 5T, K = 0.01$; Solid curve: $K < K_c$, for all other curves $K > K_c$. x is the particle distance perpendicular to the field direction. Bottom: One example of particle trajectories of Ps in the external magnetic field $B = 5$T, $n = 50$ and $K = 0.09$. The magnetic field points along the z-direction.

of the two particles. All quantities are given in atomic units. As has been discussed in [12], the Hamiltonian of Eq. (2) is not translationally invariant and the total momentum is not conserved. However, the pseudomomentum

$$\mathbf{K} = \mathbf{p}_1 + \mathbf{p}_2 - \frac{1}{2}\mathbf{B}\times\mathbf{r}_1 + \frac{1}{2}\mathbf{B}\times\mathbf{r}_2 \qquad (3)$$

is a conserved quantity. For the special case of Ps, an effective Hamiltonian is given in Cartesian coordinates(cf. Eq. 6 in [13]) by

$$H_{Ps} = \frac{1}{2\mu}\mathbf{p}^2 + \frac{\gamma}{4}(x^2+y^2) + \frac{\gamma K x}{2} + \frac{K^2}{4} - \frac{1}{\mid \mathbf{r} \mid} \qquad (4)$$

where $\mathbf{r} = \mathbf{r_1} - \mathbf{r_2}$ and $\mathbf{p} = \mathbf{p_1} - \mathbf{p_2}$ are the interparticle distance and momentum vectors. μ is the reduced mass. The magnetic field vector is $\mathbf{B} = (0,0,\gamma)$, the pseudomomentum vector $\mathbf{K} = (0,K,0)$ is assumed to point along the y axis, and $\gamma = B(\text{Tesla})/(2.35\times10^5)$. For the field strengths $B = 4T$ and $5T$ of interest here the critical values of the pseudomomentum can be calculated to be 0.061 and 0.066, respectively. In this work, we concentrate on K values around 0.1, which are above the critical values. Thus, an outer well is formed which we approximate by an anisotropic harmonic oscillator [14] and expand around the minimum. The resulting long-lived delocalized OW states are the required initial target states. Fig. 2 shows some internal coordinate distributions of the Ps ensemble, having randomly distributed starting conditions in coordinate/momentum space for different values of field strength and pseudomomentum. At the same magnetic field strength B, the internal distance $\mathbf{r}$ of Ps increases with increasing K (cf. also Fig. 1), while a stronger field and a higher internal binding energy (i.e., smaller n) compress the internal distance, in agreement with Shertzer, Ackermann and Schmelcher's work [13]. For comparison, a field-free situation is also shown.

For the incoming ensemble of projectile ions, we use a standard distribution [15]. The projectile velocity $\mathbf{v}$, its impact parameter b and the initial distance z_0 from the target determine the initial condition of the projectile. The initial distance z_0 of the projectile($\gtrsim 5\times10^4 a.u.$) is such that at this distance the projectile-Ps interaction is negligibly small compared to the electron-positron interaction. We assume that the projectile moves with a constant velocity along the z-axis, parallel to the magnetic field direction. The impact parameter of the projectile is chosen randomly by selecting b^2 in the interval $[0, b^2_{max}]$. Note that the center-of-mass motion of the Ps in the magnetic field depends on the target state. Therefore, the origin of the impact parameter $b = 0$ is estimated by calculating the meeting point of the Ps and the projectile, taking into account the projectile velocity and the center-of-mass motion of the Ps. The maximum impact parameter b_{max} is chosen sufficiently large to ensure a vanishingly small capture probability outside this b-value.

During the collision, the $\bar{p}$ projectile evolves with the approximation of a straight line trajectory under the full three-body Hamiltonian,

$$\begin{aligned} H \;=\; & \frac{1}{2}(\mathbf{p}_1+\mathbf{A}_1)^2 + \frac{1}{2}(\mathbf{p}_2-\mathbf{A}_2)^2 - \frac{1}{\mid \mathbf{r}_1-\mathbf{r}_2 \mid} \\ & + \frac{1}{\mid \mathbf{r}_1-\mathbf{r}_3 \mid} - \frac{1}{\mid \mathbf{r}_2-\mathbf{r}_3 \mid}, \end{aligned} \qquad (5)$$

where $\mathbf{r}_3$ is the coordinate of the projectile. For a given set of initial positions, the integration of Hamilton's equations of motion is performed according to Eq. (5) by a standard Runge-Kutta method.

After the collision, the projectile proceeds to an asymptotic distance ($z_f = 2\times10^5 a.u.$), sufficiently large to allow a clear energetic separation of the three particles into two-particle pairs. The resulting two-body $e^+ - e^-$ and $e^+ - \bar{p}$ energies classify the outcome of the collision: excitation or ionization of the target Ps, or capture by the projectile ion. The required two-body Hamiltonians for the electron-positron and the positron-antiproton pair, $H_{e^+-e^-}$ and $H_{e^+-\bar{p}}$, are respectively defined by:

$$H_{e^+-e^-} = \frac{1}{2}(\mathbf{p_1}+\mathbf{A_1})^2 + \frac{1}{2}(\mathbf{p_2}-\mathbf{A_2})^2 - \frac{1}{\mid \mathbf{r}_1-\mathbf{r}_2 \mid} \qquad (6)$$

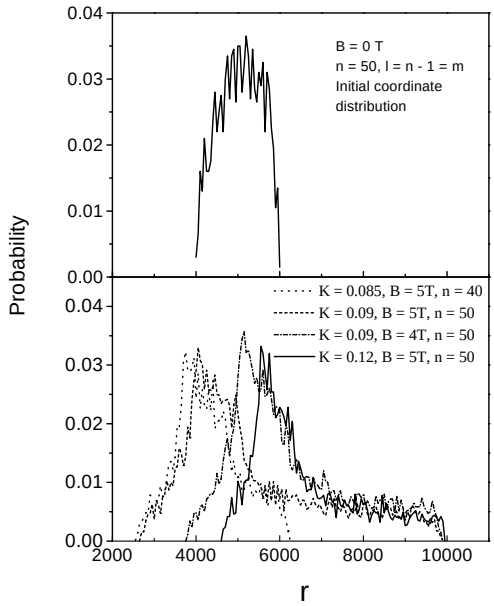

FIG. 2: Initial coordinate distribution of the positronium ensemble. Top: field-free condition (B = 0T), n = 50, l = n - 1 = m; bottom: external magnetic fields B = 4T and 5T , n = 40 and 50, K = 0.085, 0.09 and 0.12.

$$H_{e^+-\bar{p}} = \frac{1}{2}(\mathbf{p_2}-\mathbf{v})^2 - \frac{1}{|\mathbf{r}_2-\mathbf{r}_3|} + \frac{1}{2}\gamma l_z + \frac{1}{8}\gamma^2(x_2^2+y_2^2) \quad (7)$$

where l_z is the z-component of the e^+ angular momentum [6]. With Eqs. (6,7), the ionization thresholds of Ps as well as of $\bar{H}$ in the presence of a magnetic field are zero. Therefore, if $H_{e^+-e^-}$ is constant and less than zero, the positron remains bound to the e^-. If $H_{e^+-\bar{p}}$ is constant and less than zero, the positron is captured by the projectile. All other situations lead to ionization.

We now calculate the charge exchange cross-section for initial Ry states $n = 40$ and 50 of the target Ps for magnetic field strengths of 4T and 5T. The relative impact projectile velocities v_r are between 0.5 and 2.8 ($v_r = v/v_e$, with v_e the classical electron velocity in a circular Ps Bohr orbit). They correspond to collision energies between 0.62 and 19.6eV ($n = 50$) and between 0.98 and 30.6eV ($n = 40$).

The results of the charge exchange cross section are displayed in Fig. 3. To further illuminate the influence of the magnetic field, two free-field cases are also included, namely, having angular momenta $l = n-1 = m$ and $l = n-1, m = 0$ (i.e., for circular Ry motion in planes perpendicular and parallel to the z direction, respectively) [16]. The influence of the magnetic field is quite substantial: it results in a cross section reduction of a magnitude similar to the one found for $p-H$ collisions [6], the reduction being larger for increasing B. In addition, a smaller

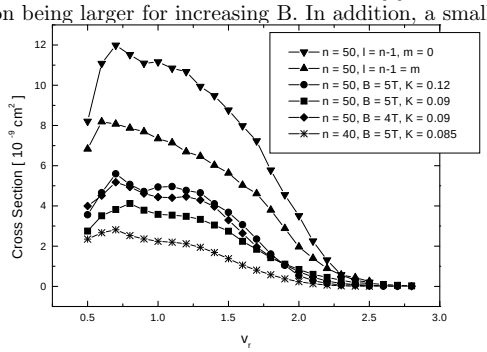

FIG. 3: Velocity-dependent charge exchange cross section for collisions of $\bar{p}$ projectiles with Ps targets in the external magnetic fields $B = 4T, 5T$ for $n = 40, 50$ and $K = 0.085, 0.09, 0.12$ initial states, respectively. For comparison, the field-free $n = 50, l = n-1 = m$ and $l = n-1, m = 0$ initial states are also included. The curves are drawn to guide the eye. Statistical uncertainty 5%.

Ps binding energy (increasing n) and a larger geometrical extension of the target Ps atom (increasing K) yields a larger capture cross section. Due to the irregular motion of the Ps (cf. Fig. 1, bottom) the velocity matching effect is not expected to play an important role. Thomas capture [17, 18], that happens in the collision plane in the field-free case [19], is foiled due to the magnetic field.

The observed behavior may be of interest for future experiments of the type $\bar{p} - e^+e^-$ or $\bar{p} - 2e^+$. Evidently, the magnetic field reduces the cross section, but this reduction remains within reasonable limits. Further explorations in the parameter space of cross section changes with K and binding energy would be worthwhile.

Acknowledgment:
We gratefully acknowledge valuable discussion with M. Zhuravlev and N. Kabachnik. This work has been supported by the Deutsche Forschungsgemeinschaft (DFG) and by the Ministry for Research and Technology (MZT) Croatia.

[1] G. Gabrielse, N. S. Bowden, P. Oxley, A. Speck, C. H. Storry, J. N. Tan, M. Wessels, D. Grzonka, W. Oelert, G. Schepers, T. Sefzick, J. Walz, H. Pittner, T. W. Hänsch, and E. A. Hessels, Phys.Rev. Lett **89** 21, 213401 (2002);

[2] G. Gabrielse, N. S. Bowden, P. Oxley, A. Speck, C. H. Storry, J. N. Tan, M. Wessels, D. Grzonka, W. Oelert, G. Schepers, T. Sefzick, J. Walz, H. Pittner, T. W. Hänsch, and E. A. Hessels, Phys.Rev. Lett **89** 23, 233401 (2002);

[3] M. Amoretti et al, Nature (London) **419**, 456 (2002);
[4] D. B. Cassidy, J. P. Merrison, M. Charlton, J. Mitray and G. Ryzhikh, J. Phys. B: At. Mol. Opt. Phys. 32, 1923(1999).
[5] J. S. Briggs and E. A. Solovév, J. Phys. B: At. Mol. Opt. Phys. 34, 1337 (2001).
[6] S. Bradenbrink, E. Y. Sidky, Z. Roller-Lutz, H. Reihl, and H. O. Lutz, Phys. Rev. A **55**, 4290 (1997);
[7] J. Lu, S. Bradenbrink, Z. Roller-Lutz, H. O. Lutz, J. Phys. B: At. Mol. Opt. Phys. **32** (1999) L681-L686; J. Lu, S. Bradenbrink, Z. Roller-Lutz, H. O. Lutz, J. Phys. B: At. Mol. Opt. Phys. **33** (2000) 2947;
[8] J. Estrada J, T. Roach, J. N. Tan, P. Yesley, G. Gabrielse, Phys.Rev. Lett **84**, 859 (2000);
[9] J. E. Avron, I. W. Herbst, and B. Simon, Ann.Phys. (N.Y.) **114**, 431 (1978);
[10] P. Schmelcher and L. S. Cederbaum, Phys. Letters **A**, 164 (1992) 305;
[11] P. Schmelcher and L. S. Cederbaum, Z. Physik **D** 24 (1992) 311;
[12] P. Schmelcher, J. Phys. **B** 25 (1992) 2697;
[13] J. Shertzer, J. Ackermann, and P. Schmelcher, Phys.Rev.A **58**, 1129 (1998);
[14] P. Schmelcher and L. S. Cederbaum, Chem. Phys. Lett.**208**, 548(1993); O. Dippel, P. Schmelcher, and L. S. Cederbaum, Phys. Rev. A **49**, 4415 (1994);
[15] R. E. Olson and A. Salop, Phys. Rev. A **16**, 531 (1977);
[16] The cross section difference between these two cases in presumably due to the so-called velocity-matching effect discussed earlier (cf. J. Lu et al., Phys. Rev. A **62**, 050701 (2000) and refs. therein): the field-free $m = 0$ state contains matching velocity components in contrast to $m = l$.
[17] L. H. Thomas, Proc. R. Soc. **114**, 561 (1927);
[18] R. Shakeshaft, L. Spruch, Rev. Mod. Phys. **51**, 369 (1979);
[19] S. Bradenbrink, H. Reihl, Z. Roller-Lutz and H. O. Lutz, J. Phys. B: At. Mol. Opt. Phys. **28**(1995), L133-L138;